Mesp2-hypomorphic fetuses (Fig. 4I,J) (Nomura-Kitabayashi et al., 2002). Fusion of proximal rib elements was also observed (Fig. 4K,L).

Mesp1/Mesp2 double-null cells cannot contribute to the formation of epithelial somites or to the dermomyotome

To address the question of whether Mesp1, in addition to Mesp2, exhibits any function during somitogenesis, we next generated Mesp1/Mesp2 double-null chimeric embryos and compared them with the Mesp2-null chimeric embryos described in the previous sections. We first performed whole-mount X-gal staining of embryos at 11 dpc. In the control chimeric embryo, the X-gal-stained Mesp1/Mesp2 double-heterozygous cells distributed randomly throughout the embryonic body, including the somite region (Fig. 5A,C). By contrast, the Mesp1/Mesp2 double-null chimeric embryo displayed a strikingly uneven pattern of cellular distribution in the somite region. The X-gal stained Mesp1/Mesp2 double-null cells were localized at the medial part of embryonic tail and were not observed in the lateral part of the somite region (Fig. 5B,D). Histological examination of parasagittal sections further revealed obvious differences in the cellular contribution to somite formation (Fig. 5E,F). In the control chimeric embryo, Mesp1/Mesp2 double-heterozygous cells distributed randomly throughout the different stages of somitogenesis (PSM, somite, dermomyotome and sclerotome; Fig. 5E). In the Mesp1/Mesp2 double-null chimeric embryo, neither the initial segment border nor epithelial somites were formed, but histologically distinguishable dermomyotome-like and sclerotome-like compartments were generated (Fig. 5F). In addition, Mesp1/Mesp2 double-null cells and wild-type cells were randomly mixed in the PSM, whereas the dermomyotome-like epithelium consisted exclusively of wild-type cells and the sclerotome-like compartment consisted mostly of Mesp1/Mesp2 double-null cells. This suggests that either Mesp1 or Mesp2 is cell-autonomously required for the formation of epithelial somite and dermomyotome. These results also indicate that PSM cells with different characteristics are rapidly sorted during somite formation.

Subsequent examination of transverse sections confirmed the elimination of Mesp1/Mesp2 double-null cells from dermomyotome (Fig. 5G,H). In the mature somite region, the wild-type dermomyotome-like epithelium was found to form the myotome (my) (Fig. 5I,J). Furthermore, the ventral part of this dermomyotome-like epithelium became mesenchymal and appeared to contribute to the dorsal sclerotome (dsc), implying that this initial dermomyotome-like epithelium actually corresponds to the epithelial somite exclusively composed of wild-type cells (Fig. 5I,J). Fluorescent phalloidin staining revealed that the apical localization of actin filaments is limited to the dorsal compartments, which are occupied by wild-type cells in the Mesp1/Mesp2 double-null chimeric embryo (Fig. 5K,L), indicating the Mesp1/Mesp2 double-null cells cannot undergo epithelialization.

It is known that the bHLH transcription factor paraxis (Tcf15 – Mouse Genome Informatics), is required for the epithelialization of somite and

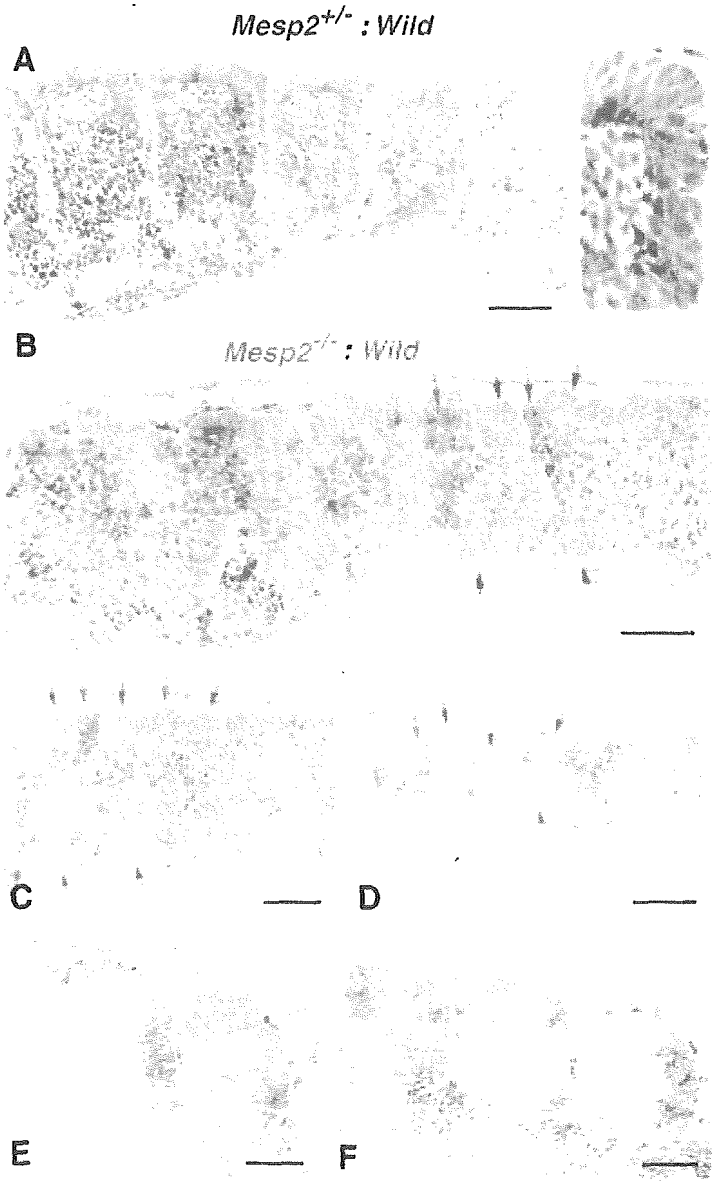

Fig. 3. Mesp2-null cells tend to be excluded from the epithelial region of the somites. (A) The control chimeric embryo undergoes normal somite formation and shows a random distribution of labeled cells. The right panel is a high-power view of a somite. (B) In the Mesp2-null chimeric embryo, incompletely segmented somites are formed. Mesp2-null cells tend to be localized at the rostral and central region of these incomplete segments. Red arrows: wild-type cell clusters; blue arrows: Mesp2-null cell clusters. (C,D) Other sections indicating multiple small epithelial cell clusters (arrows). Note that Mesp2-null cells only partially contribute to the epithelial clusters (blue arrows). (E,F) A small number of Mesp2-null cells are distributed in the dermomyotome and are mostly localized at the caudal end. Scale bars: 100 μm.

dermomyotome (Burgess et al., 1995; Burgess et al., 1996). Although *Paraxis* expression is not affected in Mesp2-null embryos (data not shown), it is possible that it is influenced by the loss of both Mesp1 and Mesp2. We therefore examined the expression patterns of *Paraxis* in our Mesp1/Mesp2 double-null chimeras. In wild-type embryos *Paraxis* is initially expressed throughout the entire somite region (in both the prospective dermomyotomal and sclerotomal regions) in the anteriormost PSM and newly forming somites, and then localizes in the dermomyotomes (Burgess et al., 1995). The dorsal dermomyotomal epithelium, composed of wild-type cells, strongly expressed *Paraxis* in the chimeric embryo (Fig. 6A,B). In addition, adjacent sections revealed that *lacZ*-expressing Mesp1/Mesp2 double-null cells expressed *Paraxis* in the medial sclerotomal compartment (Fig. 6A,B, brackets). This suggests that *Paraxis* expression in the future sclerotomal region is independent of Mesp factors. However, at present we cannot exclude the possibility that the maintenance of *Paraxis* expression in the dermomyotome requires the functions of either Mesp1 or Mesp2.

Mesp1/Mesp2 double-null cells are incapable of acquiring rostral properties

To clarify the rostro-caudal properties of somites in our chimeric embryos, we examined the expression pattern of *Uncx4.1*. Control chimeric embryos exhibited a normal stripe pattern of *Uncx4.1* expression throughout the segmented somite region (Fig. 7A). By contrast, Mesp1/Mesp2 double-null chimeric embryos exhibited continuous *Uncx4.1* expression in the ventral sclerotomal region (Fig. 7B). This continuity was observed in the entire sclerotome-like compartment of the newly formed somite region and in the ventral sclerotome in the mature somite region. The caudal localization of *Uncx4.1* expression, however, was normal in the dermomyotome and the dorsal sclerotome, which consisted of wild-type cells (Fig. 5), even in Mesp1/Mesp2 double-null chimeras. This suggests that, like Mesp2-null cells, Mesp1/Mesp2 double-null cells are incapable of acquiring rostral properties. Since the mesoderm of Mesp1/Mesp2 double-null embryos lacks the expression of the major markers of paraxial mesoderm (Kitajima et al., 2000), and Mesp1/Mesp2 double-null cells do not exhibit histological features characteristic of epithelial somites in our current study, it is possible that Mesp1/Mesp2 double-null cells may lack paraxial mesoderm properties. However, the analysis of adjacent sections suggests that *lacZ*-expressing Mesp1/Mesp2 double-null cells themselves express *Uncx4.1*, a somite-specific marker (Fig. 7C,D), and they had also been found to have normal expression of *Paraxis* (Fig. 6A,B).

It is believed that the rostro-caudal pattern within somites and dermomyotomes is generated in the PSM and maintained in somites and dermomyotomes. We observed a normal rostro-caudal pattern in the dermomyotome (Fig. 7), although wild-type cells and Mesp1/Mesp2 double-null cells are mixed in the PSM (Fig. 5), of Mesp1/Mesp2 double-null chimeric embryos. As Mesp products are required for suppression of *Dll1* in the anterior PSM, a normal Dll1 stripe pattern cannot be formed if Mesp1/Mesp2 double-null cells are randomly distributed in

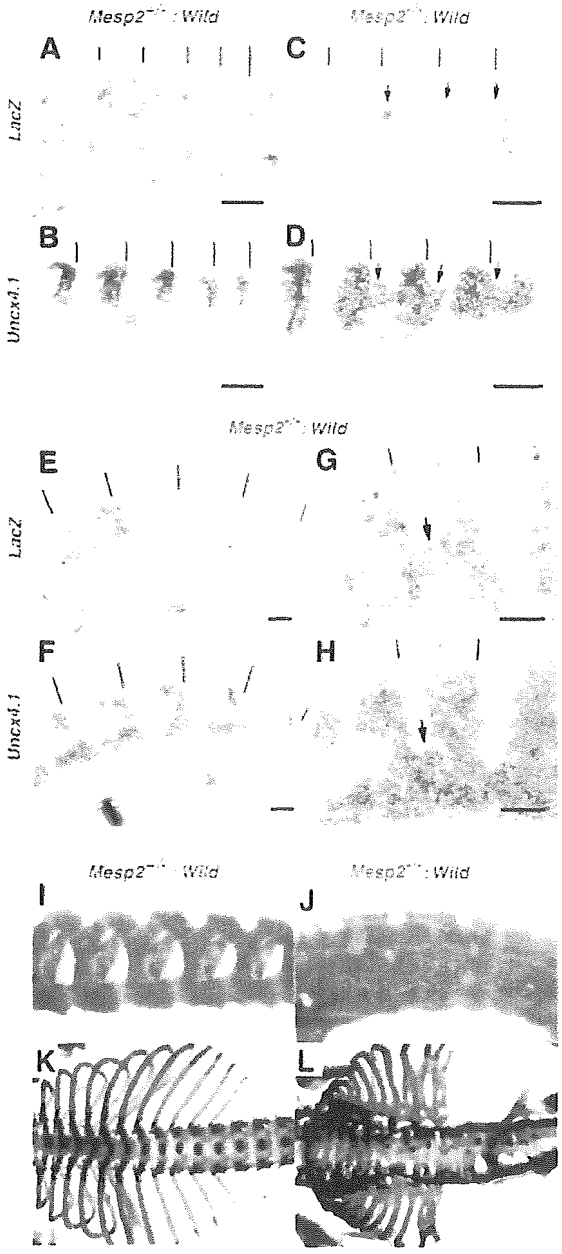

Fig. 4. Mesp2 function is cell autonomously required for rostral properties. (A-D) Expression of *lacZ* and *Uncx4.1* transcripts at the site of initial somite formation in control (A,B) and Mesp2-null (C,D) chimeric embryos. In the control, *lacZ*-expressing cells are randomly distributed and *Uncx4.1* expression is normal. In the Mesp2-null chimera, *lacZ*-expressing Mesp2-null cells at the rostral part of the incomplete segments (arrows in C) ectopically express *Uncx4.1* (arrows in D). Lines indicate somite boundaries. (E,F) In the dermomyotome, Mesp2-null cells are mostly localized at the caudal end, and the *Uncx4.1* expression pattern is normal. (G,H) In the sclerotome, the distribution of Mesp2-null cells results in expansion of *Uncx4.1* expression (arrows). (I) The control chimeric fetus shows normal vertebrae. (J) The Mesp2-null chimeric fetus exhibits partial fusion of the neural arches. (K) The control chimeric fetus shows normal ribs. (L) The Mesp2-null chimeric fetus shows proximal rib fusion. Scale bars: 100 μm. C, caudal compartment; R, rostral compartment.

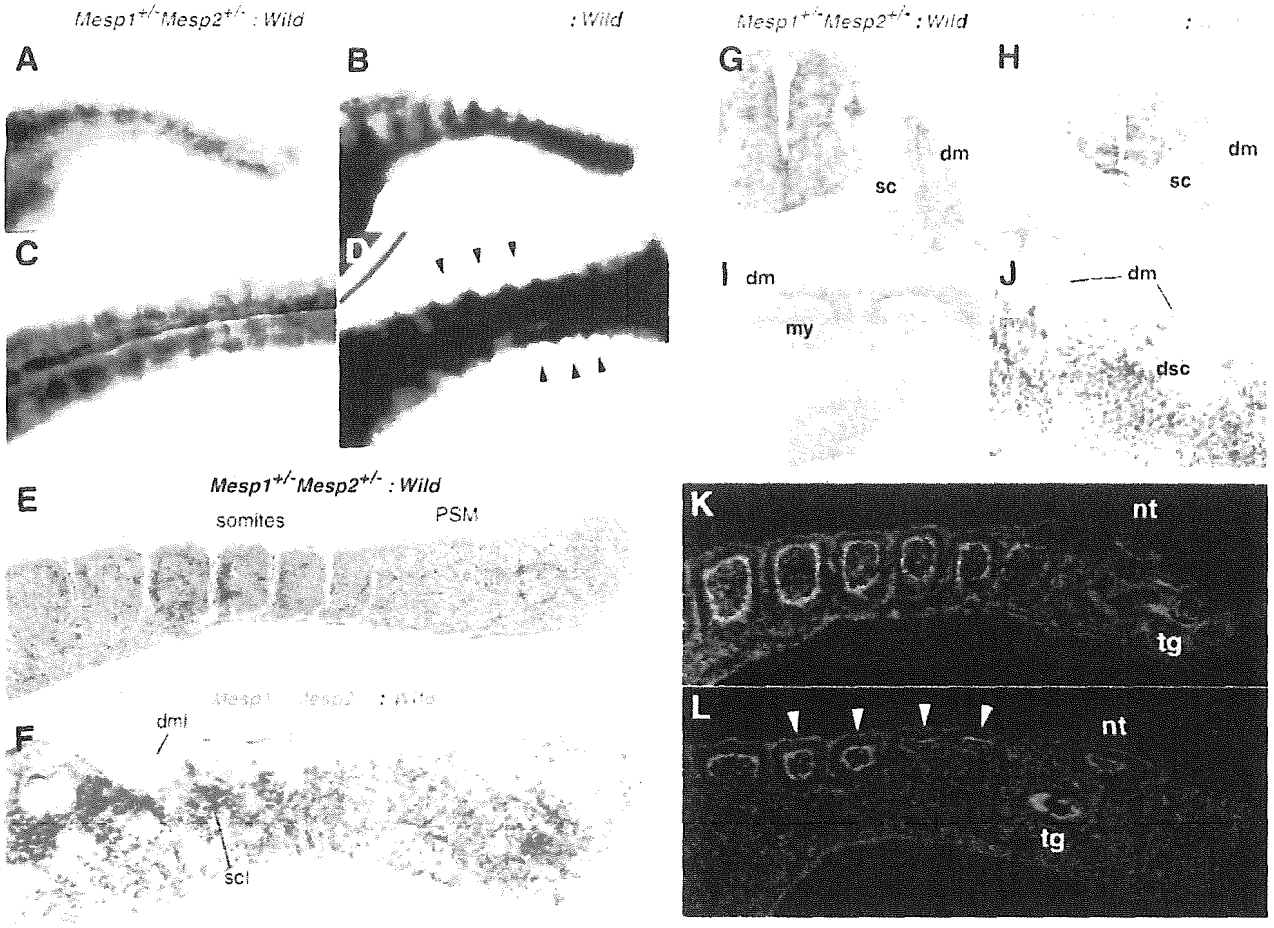

Fig. 5. Mesp1/Mesp2 double-null cells fail to contribute to epithelial somites or to the dermomyotome. (A-D) Tail regions from X-gal-stained whole-mount specimens of control (A,C) and double-null (B,D) chimeric embryos. (A,B) Lateral view. (C,D) Dorsal view. The blue double-heterozygous cells are randomly distributed in the control embryo, whereas the Mesp1/Mesp2 double-null cells are excluded from the lateral region of the somites (arrowheads in D). (E,F) Parasagittal sections of tails from chimeric embryos. (E) The labeled cells are randomly located in the control chimera. (F) The two types of cells are randomly mixed in the PSM, whereas the dermomyotome-like epithelium consisted exclusively of wild-type cells and the sclerotome-like compartment contained mostly Mesp1/Mesp2 double-null cells. Note that normal epithelial somites are not formed in this chimera. (G,H) Transverse sections show elimination of Mesp1/Mesp2 double-null cells from the dermomyotome. (I,J) The dermomyotome-like epithelium in the Mesp1/Mesp2 double-null chimeric embryo gives rise to dermomyotome, myotome (arrowhead in J) and the dorsal part of the sclerotome. Red arches indicate the inner surface of dermomyotome. (K,L) AlexaFluor 488-labeled phalloidin staining shows normal epithelialization of somites in the control chimera (K) and restriction of epithelialization in the dermomyotome-like compartment in the Mesp1/Mesp2 double-null chimera (L). dm, dermomyotome; dml, dermomyotome-like epithelium; dsc, dorsal part of the sclerotome; my, myotome; nt, neural tube; sc, sclerotome; scl, sclerotome-like compartment; tg, tail gut.

the anterior PSM. This is because 50% of cells cannot undergo suppression of Dll1 even in the future rostral half region. Therefore, our finding of a normal rostro-caudal pattern in the dermomyotome of double-null chimeras is surprising and raises the question of whether wild-type cells can be normally patterned in the presence of surrounding Mesp1/Mesp2 double-null cells. To determine how the rostro-caudal pattern in the dermomyotome is formed in the PSM, we examined the expression pattern of *Dll1* (Bettenhausen et al., 1995), the stripe expression profile of which is established in the anteriormost PSM via the function of Mesp2 (Takahashi et al., 2000). The *lacZ*-expressing Mesp1/Mesp2 double-null cells were subsequently found to be consistently localized in the sclerotome-like region, where *Dll1* expression was abnormally expanded (Fig. 6C,D). In the dermomyotome-like region, however, *Dll1* expression in the caudal half was normal. Intriguingly, strong *Dll1* expression in the anteriormost PSM was suppressed in a rostrally adjoining cell population, which is mainly occupied by wild-type cells (Fig. 6C,D, arrows). This implies that wild-type cells and Mesp1/Mesp2 double-null cells rapidly segregate at S-1 to S0, after which the rostro-caudal pattern of *Dll1* expression is formed in the partially segregated wild-type cell population but not in the randomly mixed cell population. In other words, the separation from Mesp1/Mesp2 double-null cells enabled normal rostro-caudal patterning of wild-type cells.

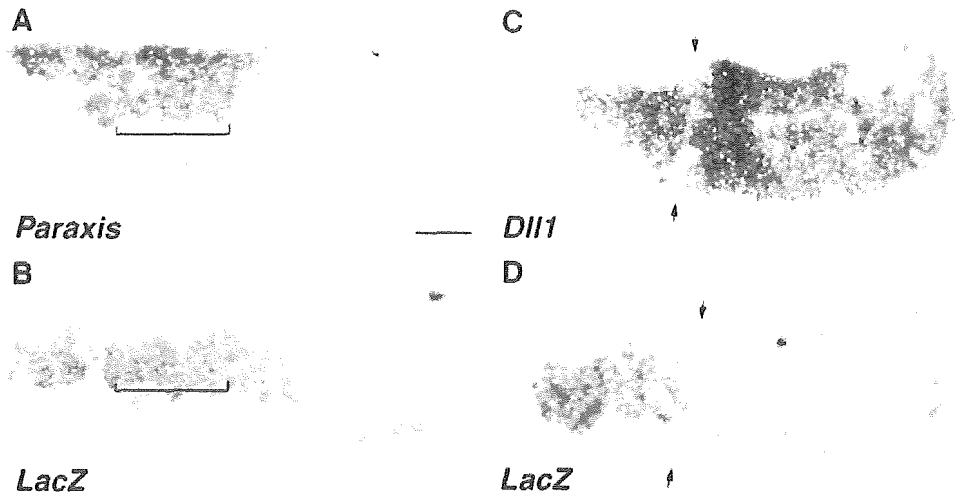

Fig. 6. (A,B) Mesp1/Mesp2 double-null cells express *Paraxis*. Adjacent parasagittal sections of the Mesp1/Mesp2 double-null chimeric embryo were stained for either *Paraxis* (A) or *lacZ* (B). Note that the expression domains of the two genes overlap in the medial sclerotomal region (brackets). (C,D) The rostro-caudal pattern in the dermomyotome is formed in a partially segregating wild-type cell population. Adjacent sections of the Mesp1/Mesp2 double-null chimeric embryos were stained for *Dll1* (C) or *lacZ* (D) mRNA. Red outlines demarcate the dorsal dermomyotome-like compartments. Note that suppression of *Dll1* expression occurs in a region mostly occupied by wild-type cells (arrows). Scale bar: 100 μm.

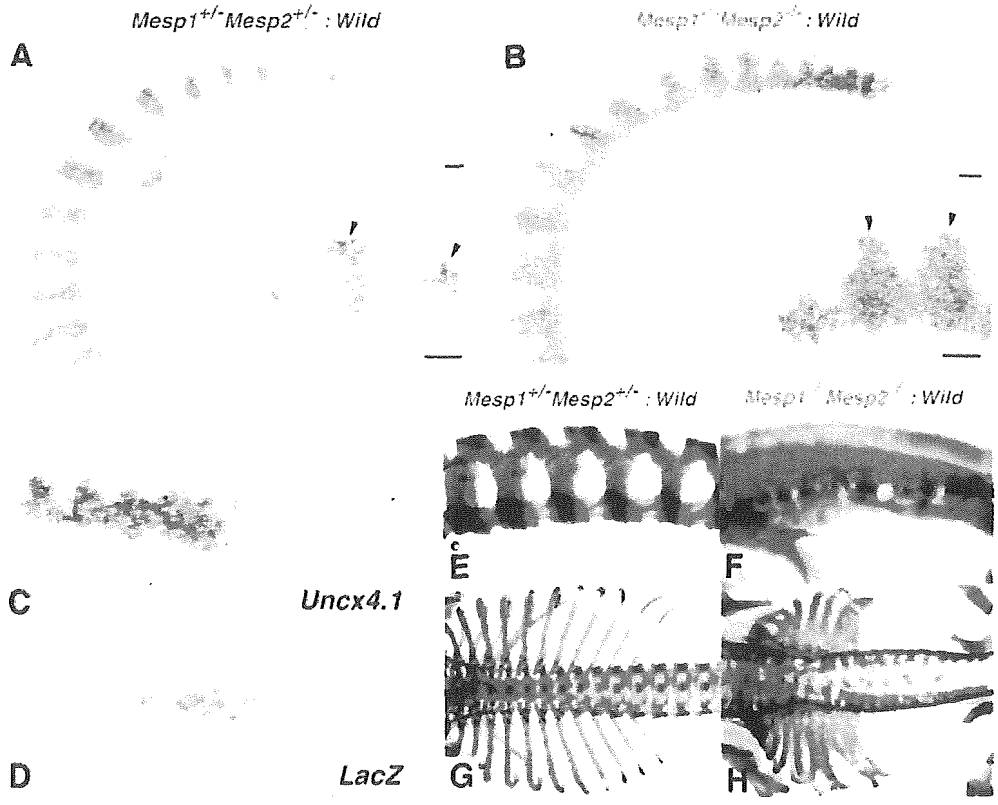

Fig. 7. Rostro-caudal patterning of the sclerotome is disrupted in Mesp1/Mesp2 double-null chimeric embryos. (A) The control chimeric embryos exhibit normal stripe patterns of *Uncx4.1* expression throughout the somite region. (B) The Mesp1/Mesp2 double-null chimeric embryos exhibit continuous *Uncx4.1* expression in the ventral sclerotomal region. Note that caudal localization of *Uncx4.1* expression is normal in the dermomyotome and dorsal sclerotome. The insets show a higher magnification of lumbar somites. (C,D) Adjacent sections showing that *lacZ*-expressing Mesp1/Mesp2 double-null cells express *Uncx4.1*. (E-H) The Mesp1/Mesp2 double-null chimeric fetus exhibits caudalization of the vertebrae and of the proximal ribs. (E) The control chimeric fetus shows normal metameric arrangement of the neural arches. (F) The Mesp1/Mesp2 double-null chimeric fetus shows severe fusion of the pedicles and the laminae of neural arches. (G) The control chimeric fetus has normal arrangement of ribs. (H) The double-null chimeric fetus shows severe fusion of the proximal elements of the ribs. Scale bars: 100 μm.

Mesp2-null fetuses display caudalized vertebrae with extensive fusion of the pedicles of neural arches and proximal elements of the ribs (Saga et al., 1997). The Mesp1/Mesp2 double-null chimeric fetuses also exhibited fusion of the pedicles of neural arches and the proximal ribs (Fig. 7E-H). Furthermore, the vertebrae of severe chimeric fetuses were indistinguishable from those of Mesp2-null fetuses. These observations indicate that Mesp1/Mesp2 double-null cells can differentiate into caudal sclerotome and possibly contribute to chondrogenesis.

Discussion

Mesp1 and Mesp2 not only exhibit similar expression patterns but also share common bHLH domains as transcription factors. Previous studies using gene replacement experiments (Saga, 1998) (Y.S. and S.K., unpublished) indicate that these genes can compensate for each other. However, the early lethality of double knockout mice hampered any further detailed analysis of somitogenesis. An obvious strategy to further elucidate the functions of Mesp1 and Mesp2 was, therefore, the generation of a conditional knockout allele for *Mesp2* in *Mesp1* disrupted cells in which the Cre gene is specifically activated in the paraxial mesoderm, which is now underway. Chimera analysis is also a powerful method as an alternative strategy. Comparisons of chimeras, composed of either Mesp2-null or Mesp1/Mesp2 double-null cells, made it possible to determine the contribution of Mesp1 to somitogenesis. Our results indicate that Mesp1 has redundant functions in the epithelialization of somitic mesoderm and additionally, by chimeric analysis, we were able to demonstrate the cell autonomy of Mesp1 and Mesp2 function during some critical steps of somitogenesis.

The relative contributions of Mesp1 and Mesp2 to somitogenesis

In Mesp1-null mice, epithelial somites with normal rostro-caudal polarity are generated, whereas Mesp2-null mice exhibit defects in both the generation of epithelial somites and the establishment of rostro-caudal polarity. Thus, it seems likely that Mesp2 function is both necessary and sufficient for somitogenesis. However, dermomyotome formation was observed, without normal segmentation, even in Mesp2-null mice. In view of the apparent redundant functions of Mesp1 and Mesp2 in somitogenesis, as demonstrated by our previous gene replacement study, it was possible that the Mesp1/Mesp2 double-null embryo would exhibit a much more severe phenotype in relation to somitogenesis. In our chimera analyses, both Mesp2-null and Mesp1/Mesp2 double-null cells exhibited complete caudalization of somitic mesoderm, indicating that Mesp1 function is not sufficient to rescue Mesp2 deficiency and restore rostro-caudal polarity. Likewise, both Mesp2-null and Mesp1/Mesp2 double-null cells were incapable of forming an initial segment boundary, showing that the contribution of Mesp1 is also minor during this process. By contrast, whereas Mesp1/Mesp2 double-null cells lacked any ability to epithelialize, Mesp2-null cells were occasionally integrated into epithelial somites and dermomyotome, indicating that the contribution of Mesp1 to epithelialization is significant and that Mesp1 can function in the absence of Mesp2 (Fig. 8). We therefore postulate that the epithelialization of dermomyotome, observed in Mesp2-null embryos, is dependent on Mesp1.

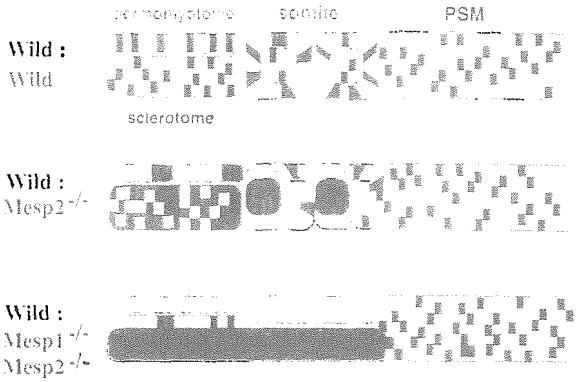

Fig. 8. A schematic summarization of the Mesp1/Mesp2 chimera experiments. Mesp1/Mesp2 double-null cells can contribute to neither epithelial somite nor dermomyotome formation, whereas Mesp2-null cells can partially contribute to both somites and dermomyotome. Red outlines indicate epithelialized tissues (epithelial somites, dermomyotomes and abnormal small clusters).

Mesp factors are cell autonomously required for epithelialization of somitic mesoderm but may also be non-cell autonomously required for morphological boundary formation

Conventional interpretations of the results of chimera analysis are generally based upon the regulative development of the vertebrate embryo and argue cell autonomy of specific gene functions in embryogenesis (Ciruna et al., 1997; Brown et al., 1999; Kitajima et al., 2000; Koizumi et al., 2001). Mesp1/Mesp2 double-null cells failed to form epithelial somites, even in the presence of surrounding wild-type cells. In addition, they were incapable of contributing to dermomyotome, where cell sorting occurs. This strongly suggests that Mesp factors are cell autonomously required for the epithelialization of somitic mesoderm. However, we also found striking non-cell autonomous effects of Mesp mutant cells on wild-type cell behaviors. That is, both types of Mesp mutant cell not only failed to undergo normal somitogenesis, but also inhibited the normal morphogenesis of wild-type cells. This implies that there are non-cell autonomous roles for Mesp factors in the establishment of the future somite boundary, as we will discuss further.

Initial epithelial somite formation is achieved by the mesenchymal-epithelial transition of cells located in the anterior PSM. A future somite boundary is established at a specific position in the PSM, followed by gap formation between the mesenchymal cell populations. Subsequently, cells located anterior to the boundary are epithelialized. This process is known to be mediated by an inductive signal from cells posterior to the boundary (Sato et al., 2002). Therefore, defects in epithelial somite formation can be explained in two principal ways: a lack of cellular ability to epithelialize (cell autonomous) and a lack of an inducing signal, which is produced in the anterior PSM by a mechanism mediated by Notch signaling (thus non-cell autonomous). In the case of chimeras of Mesp1/Mesp2 double-null cells, no local

boundary formed by locally distributed wild-type cells was observed, i.e. even a gap between wild-type cells was never observed in the mixture of Mesp1/Mesp2 double-null cells and wild-type cells. It is likely, therefore, that the wild-type cell population can form a boundary only after separation from Mesp1/Mesp2 double-null cells (Fig. 8). By contrast, some local boundaries between epithelial wild-type cell clusters were occasionally observed in chimeras with Mesp2-null cells. Considering that there is functional redundancy between these transcription factors, it is possible that either Mesp1 or Mesp2 is necessary for the formation of a signaling center or source of the putative inductive signal. Hence, we cannot exclude the possibility that the lack of Mesp function may affect non-cell autonomous generation of the inductive signal in the anterior PSM.

Formation of epithelial somites requires paraxis, which is a transcription factor (Burgess et al., 1996; Nakaya et al., 2004). We observed that Mesp1/Mesp2 double-null cells at the medial sclerotomal region expressed *Paraxis*, indicating that Mesp factors are not absolutely required for *Paraxis* expression. Defects in epithelial somite formation in paraxis-null embryos, with normal *Mesp2* expression (Johnson et al., 2001), and in Mesp2-null embryos, with normal *Paraxis* expression, imply that epithelial somite formation independently requires both gene functions.

Mesp2 is cell autonomously required for the acquisition of rostral properties

The distribution of Mesp2-null cells in the Mesp2-null chimeric embryos may appear somewhat paradoxical, as they are localized at the rostral side in the incomplete somites but at the caudal side in the dermomyotome. Initial localization at the rostral and central region, however, is likely to be due to the relative lack of epithelialization functions. In mammalian and avian embryos, mesenchymal-to-epithelial conversion of the PSM commences from the rostral side of the future somite boundary, i.e. the caudal margin of the presumptive somite (Duband et al., 1987). Epithelialization then proceeds anteriorly in the dorsal and ventral faces and in such a process, Mesp2-null cells, which are less able to participate in epithelialization, may therefore be pushed to the central and rostral sides. Thus, the majority of the Mesp2-null cells localize to the central, prospective sclerotomal region and a small number of them are integrated in the future dermomyotomal region. The incomplete somites then undergo reorganization into dermomyotome and sclerotome, and small numbers of Mesp2-null cells in the dermomyotome may be sorted out to the caudal end. Therefore, the apparently complex distribution pattern of Mesp2-null cells is likely to reflect a combination of defects in epithelialization and rostro-caudal patterning. In the incomplete segments of Mesp2-null chimeric embryos, the Mesp2-null cells fail to acquire rostral properties even when localized at the rostral side. Moreover, in the dermomyotome, where rostro-caudal patterning is rescued, Mesp2-null cells are mostly localized in the caudal region. These observations suggested that the requirement of Mesp2 for the acquisition of rostral properties is cell autonomous. Similarly, it has been reported that presenilin 1 (Psen1) is required for acquisition of caudal half properties (Takahashi et al., 2000; Koizumi et al., 2001) and that Psen1-null cells cannot contribute to the caudal half of somites in chimeric embryos, showing cell autonomous roles for Psen1 (Koizumi et al., 2001).

Mesp mutant cells affect the rostro-caudal patterning of somites due to the lack of cellular interaction with wild-type cells

In a previous study, we have shown that the rostro-caudal patterning of somites is generated by complex cellular interactions involved in positive and negative feedback pathways of Dll1-Notch and Dll3-Notch signaling, and regulation by Mesp2 in the PSM (Takahashi et al., 2003). In chimeras with either Mesp2-null or Mesp1/Mesp2 double-null cells, the mutant cells were distributed evenly and did not show any sorting bias in a rostro-caudal direction in the PSM. Since both Mesp2-null and Mesp1/Mesp2 double-null cells have the ability to form caudal cells, it is likely that if wild-type cells could occupy the rostral part of future somite regions and have the ability to sort in the PSM, a normal rostro-caudal patterning would be generated. We did not observe this, however, and conclude that the presence of mutant cells lacking Mesp factors must have disrupted normal cellular interactions via Notch signaling. Thus these non-cell-autonomous effects of our mutant cells are strongly supportive of our previous contention that rostro-caudal pattering is generated by cellular interactions via Notch signaling.

We thank Mariko Ikumi, Seiko Shinzawa, Eriko Ikeno and Shinobu Watanabe for general technical assistance. This work was supported by Grants-in-Aid for Science Research on Priority Areas (B) and the Organized Research Combination System of the Ministry of Education, Culture, Sports, Science and Technology, Japan.

References

Bettenhausen, B., Hrabe de Angelis, M., Simon, D., Guénet, J.-L. and Gossler, A. (1995). Transient and restricted expression during mouse embryogenesis of Dll1, a murine gene closely related to *Drosophila* Delta. *Development* **121**, 2407-2418.

Borycki, A. G. and Emerson, C. P., Jr (2000). Multiple tissue interactions and signal transduction pathways control somite myogenesis. *Curr. Top. Dev. Biol.* **48**, 165-224.

Brown, D., Wagner, D., Li, X., Richardson, D. A. and Olson, E. N. (1999). Dual role of the basic helix-loop-helix transcription factor scleraxis in mesoderm formation and chondrogenesis during mouse embryogenesis. *Development* **126**, 4317-4329.

Burgess, R., Cserjesi, P., Ligon, K. L. and Olson, E. N. (1995). Paraxis: a basic helix-loop-helix protein expressed in paraxial mesoderm and developing somites. *Dev. Biol.* **168**, 296-306.

Burgess, R., Rawls, A., Brown, D., Bradley, A. and Olson, E. N. (1996). Requirement of the *paraxis* gene for somite formation and musculoskeletal patterning. *Nature* **384**, 570-573.

Ciruna, B. G., Schwartz, L., Harpal, K., Yamaguchi, T. P. and Rossant, J. (1997). Chimeric analysis of *fibroblast growth factor receptor-1 (Fgfr1)* function: a role for FGFR1 in morphogenetic movement through the primitive streak. *Development* **124**, 2829-2841.

Duband, J. L., Dufour, S., Hatta, K., Takeichi, M., Edelman, G. M. and Thiery, J. P. (1987). Adhesion molecules during somitogenesis in the avian embryo. *J. Cell Biol.* **104**, 1361-1374.

Fan, C. M. and Tessier Lavigne, M. (1994). Patterning of mammalian somites by surface ectoderm and notochord: Evidence for sclerotome induction by a hedgehog homolog. *Cell* **79**, 1175-1186.

Gossler, A. and Hrabe de Angelis, M. (1997). Somitogenesis. *Curr. Top. Dev. Biol.* **38**, 225-287.

Johnson, J., Rhee, J., Parsons, S. M., Brown, D., Olson, E. N. and Rawls, A. (2001). The anterior/posterior polarity of somites is disrupted in Paraxis-deficient mice. *Dev. Biol.* **229**, 176-187.

Kitajima, S., Takagi, A., Inoue, T. and Saga, Y. (2000). MesP1 and MesP2

are essential for the development of cardiac mesoderm. *Development* **127**, 3215-3226.

Koizumi, K., Nakajima, M., Yuasa, S., Saga, Y., Sakai, T., Kuriyama, T., Shirasawa, T. and Koseki, H. (2001). The role of presenilin 1 during somite segmentation. *Development* **128**, 1391-1402.

Mansouri, A., Yokota, Y., Wehr, R., Copeland, N. G., Jenkins, N. A. and Gruss, P. (1997). Paired-related murine homeobox gene expressed in the developing sclerotome, kidney, and nervous system. *Dev. Dyn.* **210**, 53-65.

Nakaya, Y., Kuroda, S., Katagiri, Y. T., Kaibuchi, K. and Takahashi, Y. (2004). Mesenchymal-epithelial transition during somitic segmentation is regulated by differential roles of Cdc42 and Rac1. *Dev. Cell* **7**, 425-438.

Neidhardt, L. M., Kispert, A. and Herrmann, B. G. (1997). A mouse gene of the paired-related homeobox class expressed in the caudal somite compartment and in the developing vertebral column, kidney and nervous system. *Dev. Genes Evol.* **207**, 330-339.

Nieto, M. A., Gilardi-Hebenstreit, P., Charnay, P. and Wilkinson, D. G. (1992). A receptor protein tyrosine kinase implicated in the segmental patterning of the hindbrain and mesoderm. *Development* **116**, 1137-1150.

Nomura-Kitabayashi, A., Takahashi, Y., Kitajima, S., Inoue, T., Takeda, H. and Saga, Y. (2002). Hypomorphic *Mesp* allele distinguishes establishment of rostro-caudal polarity and segment border formation in somitogenesis. *Development* **129**, 2473-2481.

Pourquié, O. (2001). Vertebrate somitogenesis. *Annu. Rev. Cell. Dev. Biol.* **17**, 311-350.

Saga, Y. (1998). Genetic rescue of segmentation defect in MesP2-deficient mice by MesP1 gene replacement. *Mech. Dev.* **75**, 53-66.

Saga, Y. and Takeda, H. (2001). The making of the somite: molecular events in vertebrate segmentation. *Nat. Rev. Genet.* **2**, 835-845.

Saga, Y., Hata, N., Kobayashi, S., Magnuson, T., Seldin, M. and Taketo, M. M. (1996). MesP1: A novel basic helix-loop-helix protein expressed in the nascent mesodermal cells during mouse gastrulation. *Development* **122**, 2769-2778.

Saga, Y., Hata, N., Koseki, H. and Taketo, M. M. (1997). *Mesp2*: a novel mouse gene expressed in the presegmented mesoderm and essential for segmentation initiation. *Genes Dev.* **11**, 1827-1839.

Saga, Y., Miyagawa-Tomita, S., Takagi, A., Kitajima S., Miyazaki, J. and Inoue, T (1999). MesP1 is expressed in the heart precursor cells and required for the formation of a single heart tube. *Development* **126**, 3437-3447.

Sato, Y., Yasuda, K. and Takahashi, Y. (2002). Morphological boundary forms by a novel inductive event mediated by Lunatic fringe and Notch during somitic segmentation. *Development* **129**, 3633-3644.

Takahashi, Y., Koizumi, K., Takagi, A., Kitajima, S., Inoue, T., Koseki, H. and Saga, Y. (2000). Mesp2 initiates somite segmentation through the Notch signalling pathway. *Nat. Genet.* **25**, 390-396.

Takahashi, Y., Inoue, T., Gossler, A. and Saga, Y. (2003). Feedback loops comprising Dll1, Dll3 and Mesp2, and differential involvement of Psen1 are essential for rostrocaudal patterning of somites. *Development* **130**, 4259-4268.

Zambrowicz, B. P., Imamoto, A., Fiering, S., Herzenberg, L. A., Kerr, W. G. and Soriano, P. (1997). Disruption of overlapping transcripts in the ROSA beta geo 26 gene trap strain leads to widespread expression of beta-galactosidase in mouse embryos and hematopoietic cells. *Proc. Natl. Acad. Sci. USA* **94**, 3789-3794.

American Journal of Pathology, Vol. 165, No. 6, December 2004

Vascular Biology, Atherosclerosis and Endothelium Biology

E4F1, a Novel Estrogen-Responsive Gene in Possible Atheroprotection, Revealed by Microarray Analysis

Yasuhiro Nakamura,*† Katsuhide Igarashi,‡ Takashi Suzuki,* Jun Kanno,‡ Tohru Inoue,§ Chika Tazawa,* Masayuki Saruta,* Tomoko Ando,‡ Noriko Moriyama,‡ Toru Furukawa,¶ Masao Ono,* Takuya Moriya,* Kiyoshi Ito,‖ Haruo Saito,† Tadashi Ishibashi,† Shoki Takahashi,† Shogo Yamada,† and Hironobu Sasano*

From the Departments of Pathology, Radiology,† Molecular Pathology,¶ and Gynecology,‖ Tohoku University School of Medicine, Sendai; and the Division of Toxicology‡ and the Biological Safety Research Center,§ National Institute of Health Sciences, Tokyo, Japan*

Estrogen has been postulated to be involved in inhibition of vascular smooth muscle cell (VSMC) proliferation mainly via estrogen receptor (ER), but the detailed mechanism has remained primarily unknown. Therefore, in this study, microarray analysis was used in two types of cultured human VSMCs: one positive for ERα, and the other for ERβ, which were treated by estrogens to detect the estrogen-responsive genes. We also used quantitative reverse transcriptase-polymerase chain reaction (RT-PCR) to evaluate mRNA levels of selective target gene (TG) in these cells. We further studied whether the TG product was involved in inhibition of proliferation using small interfering RNA (siRNA) of the TG transfection. We subsequently used quantitative RT-PCR and *in situ* hybridization analysis to evaluate the expression of these gene products in human aorta. E4F1, a possible inducer of cell growth arrest, was markedly increased only in ERα-positive VSMCs by estrogens in both microarray and RT-PCR analyses. Blocking of E4F1 using siRNA suppressed estrogenic inhibition of ERα-positive VSMC proliferation. E4F1 mRNA was abundant in premenopausal female aorta with mild atherosclerotic changes. E4F1 is therefore considered one of the estrogen-responsive genes involving ERα-mediated inhibition of VSMC proliferation and may play an important role in estrogen-related atheroprotection of human aorta. ***(Am J Pathol 2004, 165:2019–2031)***

Estrogen has been proposed as a cardioprotective agent.[1] However it is also true that the significance of hormone replacement therapy has remained controversial because recent randomized controlled trials failed to show protective effects of hormone replacement therapy in reducing the risk of coronary artery disease and instead revealed undesirable side effects such as an increment of breast cancer incidence.[2–4] Results of experimental, clinical, and epidemiological studies have, however, also demonstrated that estrogen is predominantly involved in the suppression of development of atherosclerosis.[2,5,6] Therefore, it is still very important to examine the detailed mechanisms of estrogenic actions especially in relation to its atheroprotective effects in the human cardiovascular system.

Estrogens have been considered to exert direct antiatherogenic effects through an initial interaction with estrogen receptor (ER) in vascular smooth muscle cells (VSMCs) in addition to various systemic estrogenic effects. Results of recent studies demonstrated that there are two subtypes of ERs, ERα and ERβ.[7,8] The presence of both ERα and ERβ has been also reported in the vascular wall of cardiovascular systems in human and various experimental animals.[9] Between both ERs, ERα has been considered to be important for anti-atherogenic effects of estrogen in the great majority of the cases.[9–13] However, the detailed genomic mechanisms of estrogen-ERα actions in inhibition of VSMC proliferation remain virtually unknown. Especially the target gene (TG) induced by estrogen, ie, estrogen-responsive gene, has not been examined in the human cardiovascular system.

Supported in part by Health and Labor Sciences Research Grants for Risk Analysis Research on Food and Pharmaceuticals (H13-Seikatsu-013) from the Ministry of Health, Labor, and Welfare of Japan.

Accepted for publication August 25, 2004.

Address reprint requests to Yasuhiro Nakamura, M.D., Department of Pathology, Tohoku University School of Medicine, 2-1 Seiryo-machi, Aoba-ku, Sendai, 980- 8575 Japan. E-mail: nakamura@patholo2.med.tohoku.ac.jp.

Table 1. Primer Sequences Used in RT-PCR Analysis for VSMC Characterization

cDNA	Sequence	Size (bp)	Reference no.
ERα	Forward 5′-AAGAGCTGCCAGGCCTGCC-3′ Reverse 5′-TTGGCAGCTCTCATGTCTCC-3′	167	56
ERβ	Forward 5′-GCTCAATTCCAGTATGTA-3′ Reverse 5′-CCTGGTGTAAAAACGTGA-3′	241	57
GAPDH	Forward 5′-TGAACGGGAAGCTCACTGG-3′ Reverse 5′-TCCACCACCCTGTTGCTGTA-3′	307	58

Recently, expression profiling analysis using cDNA microarray technology has been demonstrated to provide very important information as to the elucidation of the scheme of estrogen-signaling and improvement of clinical decisions in ERα-positive breast cancer.[14] A number of investigators also identified several novel estrogen-responsive genes using a cDNA microarray method in other tissues and cancer cells.[14,15] However, there has been little information regarding estrogen-responsive genes involving anti-atherogenic effects induced by estrogens in the human cardiovascular system. Therefore, in this study, we first screened the estrogen-responsive gene involving inhibition of VSMC proliferation using a microarray in a cell line derived from ERα-positive human VSMCs. We then used quantitative reverse transcriptase-polymerase chain reaction (RT-PCR) to evaluate the expression level of this TG mRNA in both dose- and time-dependent manners to further confirm the results of microarray analysis. We also examined whether the TG detected in ERα-positive VSMCs can be also induced by estrogens in ERβ-positive VSMCs. Double-stranded RNAs (dsRNAs) have been recently reported to be remarkably effective at suppressing specific gene expression in various kinds of cells by a pathway involving RNA interference (RNAi) through small interfering RNAs (siRNAs).[16–18] Therefore, we used this procedure to confirm whether the gene products derived from the TG detected in microarray analysis were associated with estrogenic inhibition of cell proliferation in ERα-positive cells.

It then becomes very important to study the expression of the genes detected by microarray analysis in human VSMCs to obtain their clinical relevance. We therefore examined the expression levels of the above TG in VSMCs of human abdominal aorta obtained by autopsy using both quantitative RT-PCR and the *in situ* hybridization method. We then correlated these findings with the degree of atherosclerosis, sex, ERα expression levels, and other features of the patients for further characterization of the findings.

Materials and Methods

Cell Culture and Characterization

Two types of human VSMCs, ie, HUVS-112D (derived from human umbilical cord; CRL-2481), and T/G HA-VSMC (derived from human aorta; CRL-1999) were commercially obtained from American Type Culture Collection (Manassas, VA). They were cultured in a 75-cm^2 flask with F12-K medium (American Type Culture Collection) containing 5% fetal bovine serum (FBS) at 37°C in a 5% CO_2 atmosphere. We first characterized these cell lines using several methods, such as morphological, immunohistochemical, and microarray analyses described below. In addition, we examined whether these cells expressed both ERs, especially ERα, using quantitative RT-PCR and Western blot analysis in combination with semiquantification, as described below.

Quantitative RT-PCR

Total RNA was extracted from both VSMCs in 1 ml of TRIzol reagent (Invitrogen, Carlsbad, CA) followed by a phenol-chloroform phase extraction and isopropanol precipitation. The Superscript Preamplification System RT kit (Life Technologies, Inc., Grand Island, NY) was used in the synthesis and amplification of complementary DNA (cDNA). cDNA was synthesized from total RNA (2 μg) using 25 ng/μL of Oligo $(dT)_{12-18}$ Primer (Life Technologies Inc., Gaithersburg, MD) on a PTC-200 Peltier thermal cycler DNA engine (MJ Research Inc., Watertown, MA). To test for the presence of genomic DNA contamination, we performed the RT step in the absence of Superscript II RNase H^- reverse transcriptase (Life Technologies, Inc.) followed by PCR. RT-PCR products lacking reverse transcriptase in the initial RT step were run on an ethidium bromide-stained 2% agarose gel. No band was observed in these samples (data not shown). The resulting cDNA was used as a template for real-time PCR. Real-time PCR was performed with the Light Cycler System (Roche Diagnostics GmbH, Mannheim, Germany) using the DNA binding dye SYBR Green I (Roche Diagnostics GmbH) for the detection of PCR products. Primers are summarized in Table 1. As a positive control, T-47D human breast cancer cells were used for ERα and ERβ.[19] Negative control experiments lacked cDNA substrate to check for the presence of exogenous contaminant DNA. No amplified products were detected under these conditions. The mRNA levels for both ERs in each VSMC are summarized as a ratio of glyceraldehyde-3-phosphate dehydrogenase (GAPDH), and evaluated as a ratio (%) compared with that of each control cDNA, which were synthesized from each PCR products and purified by using the pGEM-T Easy vector. The detailed procedures above were previously described in detail.[20] The analyses with real-time PCR were triplicated.

Western Blot Analysis

The procedures were based on these reported previously.[21] The above VSMCs were washed with ice-cold phosphate-buffered saline (PBS) and then lysed in a triple detergent buffer containing 50 mmol/L Tris-HCl (pH 8.0), 150 mmol/L NaCl, 0.02% sodium azide, 0.1% sodium dodecyl sulfate, 100 μg/ml phenylmethyl sulfonyl fluoride, 1 μg/ml aprotin, 1% Nonidet P-40, and 0.5% sodium deoxycholate. A Protein Assay Rapid Kit (Wako, Osaka, Japan) and a SpectraMax 190 microplate reader (Molecular Devices Corp., Sunnyvale, CA) were used to determine the concentration of protein according to the manufacturers' instructions. A Western blot analysis was performed using 60 μg of each protein. After optimizing the conditions of experiments, 60 μg of protein samples were denatured at 95°C in Tris/glycine/sodium dodecyl sulfate buffer (25 mmol/L Tris, 192 mmol/L glycine, 0.1% sodium dodecyl sulfate, pH 8.3) and electrophoresed at 25-mA constant current through a 10 to 20% polyacrylamide gradient gel (Bio-Rad, Hercules, CA). The proteins in the gel were electrophoretically transferred to a polyvinylidene difluoride membrane (Clear Blot Membrane-P; ATTO Co. Ltd., Tokyo, Japan). Nonspecific binding sites were blocked by immersing the membrane in 5% skim milk (Becton Dickinson and Company, NJ) for 1 hour at room temperature, washed twice in 0.05% Tween 20 and PBS (PBS-T), and then incubated with ERα polyclonal antibody (Santa Cruz Biotechnology, Inc., Santa Cruz, CA) or control IgG overnight at 4°C. After washing in PBS-T, membranes were incubated for 1 hour with horseradish peroxidase-conjugated anti-mouse IgG (Amersham), and the target protein was detected using the ECL Western blotting detection reagent (Amersham). Equal loading of protein in each lane was confirmed by probing the membrane with anti-human β-actin monoclonal antibody (Sigma, St. Louis, MO). The relative amounts of ERα and β-actin protein levels for each band were standardized to the relative OD units obtained by an Image Gauge system (Fuji Photo Film Co. Ltd., Minamishinagawa, Kanagawa, Japan). In addition, the relative amount of ERα protein was adjusted by the β-actin protein level, and then evaluated as a ratio (%) to untreated MCF-7 cell lines.[22] The analyses were also triplicated.

GeneChip Microarray Assay

Estrogen Treatment

The two types of VSMC cells described above were seeded in a 75-cm^2 flask at an initial concentration of 100,000 cells/flask with F12-K medium (American Type Culture Collection) containing 5% FBS and cultured until a subconfluent state was obtained. The medium was then replaced with FBS-free and phenol red-free medium (modified Eagle's medium) (Sigma) to arrest the cell growth. After 24 hours, the medium was replaced again with phenol red-free and FBS-free medium in the presence of estrogen (10 nmol/L) or vehicle (0.1% ethanol). After incubation for 8 hours, the cells were subsequently subjected to total RNA extraction for microarray analysis. Total RNA was prepared using TRIzol reagent (Invitrogen) according to the manufacturer's instructions. RNA was further purified using RNeasy columns (Qiagen, Valencia, CA) and treatment with ribonuclease-free deoxyribonuclease I (Qiagen).

Labeling

Isolated total RNA was labeled as described in the Affymetrix (Santa Clara, CA) GeneChip Expression Analysis Technical Manual (revision 3). The labeling is performed in two steps. In the first step, double-stranded cDNAs (ds-cDNAs) were synthesized from total RNA by reverse transcriptase reaction with SuperScript Reverse Transcriptase II (Life Technologies) and an oligo (dT) primer linked to a T7 RNA polymerase-binding site sequence and second strand synthesis reaction with *Escherichia coli* DNA polymerase, DNA ligase, and RNaseH. In the second step, the resulted ds-cDNAs were used as templates to produce biotin-labeled cRNA (the target) using T7 RNA polymerase in the presence of biotinylated UTP and CTP (Enzo Diagnostics, Farmingdale, NY). The biotin-labeled cRNAs were fragmented in fragmentation buffer and used for the preparation of target solution.

GeneChip Genome Array Hybridization

Fragmented targets are combined with control oligomer (Control Oligo B2, Affymetrix) and control cRNAs (Eukaryotic Hybridization Control kit, Affymetrix) in a hybridization buffer (100 mmol/L MES, 1 mol/L Na^+, 20 mmol/L ethylenediaminetetraacetic acid, 0.01% Tween 20). Each target was hybridized to HGU133A using protocols described in the Affymetrix Expression Analysis Technical Manual.

Data Analysis

The procedure was basically based on the previously reported study.[23] The fluorescent signals on the slides were scanned by a GeneArray scanner (Affymetrix) and further data processing was performed using Microsoft Excel software (Microsoft, Seattle, WA). Image analysis was performed using Microarray Suite 5.0 software (Affymetrix). In this study, the ratios represented the values changed by 10 nmol/L E_2 treatment compared to control values. The values obtained from each experiment were log transformed and normalized so that the median log-transformed ratio equaled zero. To confirm the estrogen-related changes in gene expression obtained from microarray analysis, we independently repeated the same experiment twice and the differences were calculated. To further maintain reproducibility, we also selected for further analysis only those genes in which the difference of expression levels at the same condition in two separate experiments did not exceed more than 2.5-fold in further analysis. The average ratios yielded by these independent experiments were then used to denote the gene expression levels. As the average ratios increased more than twofold by both of duplicated 10 nmol/L E_2 treatment

Table 2. The Sequence Information of Primers, siRNA, and Probes for *in Situ* hybridization for Target Gene (E4F1)

Primers for RT-PCR	Forward	5′-ACACCACACAGGCGAGAA-3′
	Reverse	5′-TCCTCAGACACCAGCAACT-3′
Gene-specific sequences for siRNA	Sense	5′- AAGCTCTACAAGACCATTGCC-3′
	Anti-sense	5′-AAGCTCTACAAGACCATTGCC-3′
Gene-specific probes for *in situ* hybridization	Anti-sense	5′-CCACGGAGATCATCGAGGGCACCCAGACAGAGGTGGACAGCCACATCATG-3′
	Sense	5′-CATGATGTGGCTGTCCACCTCTGTCTGGGTGCCCTCGATGATCTCCGTGG-3′

It was determined that the target gene in this study was E4F1 by microarray analysis. The reason for this determination was described in detail in the Results section.

were considered to have been up-regulated when compared to control values. In this study, among the genes detected in microarray analysis, we regarded a gene that was up-regulated and was significantly associated with inhibition of cell growth in ERα-positive cells as the TG in this study. In an analysis of the function of these detected genes, we used the homepage of HUGO Human Gene Nomenclature Committee (*http://www.gene.ucl.ac.uk/nomenclature/*) for further clarification. We then examined whether there was an estrogen-responsive element (ERE) in the promoter region of TG by analyzing 10,000 bp upstream of the transcription start sites for TG with sequence information of chromosome mapping provided by the above homepage.

Real-Time PCR for TG mRNA

Estrogen Treatment

The ERα-positive cells were seeded in a 75-cm^2 flask at an initial concentration of 100,000 cells/flask with F-12K medium containing 5% FBS and cultured until a subconfluent state was obtained. The medium was then replaced with phenol red-free and FBS-free medium to arrest the cell growth. After 24 hours, the medium was replaced again with FBS-free F12-K medium with E_2 (100 pmol/L, 10 nmol/L), E_2 (10 nmol/L) with ICI 182780 (1 μmol/L; Tocris, Ballwin, MO), tamoxifen (TAM, Sigma) alone (10 nmol/L), raloxifene (RAL, Sigma) alone (10 nmol/L), or vehicle. In addition, after pretreatment of the cells with inhibitors of RNA transcription, actinomycin D (ACD) (1 μmol/L, Sigma), or protein translation (Sigma), cycloheximide (CHX) (1 μmol/L, ICN Biomedicals Inc.), other two flasks were replaced again with FBS-free medium with E_2 (10 nmol/L). After incubation for 8 hours, the cells were subsequently subjected to total RNA extraction for real-time RT-PCR analysis described above for target product mRNA expression. In addition, the cells were also incubated for 24 hours and 48 hours, respectively, with E_2 alone (10 nmol/L) or vehicle and also subsequently subjected to total RNA extraction for real-time RT-PCR analysis described above for expression levels of TG product mRNA. The mRNA levels for target product in each VSMC are summarized as a ratio of GAPDH, and evaluated as a ratio (%) compared with that of each control cDNA, which were synthesized from each PCR product and purified by using the pGEM-T Easy vector. The procedures were also previously described in detail.[20] As a contrast, we also examined the relative expression levels of TG products mRNA treated with E_2 (100 pmol/L, 10 nmol/L) or vehicle for 8 hours, and treated with E_2 (10 nmol/L) or vehicle for 24 hours and 48 hours in ERβ-positive cells. The analyses with real-time PCR were triplicated by using three flasks per treatment or nontreatment. The sequence information of primers for TG is shown in Table 2.

siRNA Preparation, Transfection, and Cell Count Assay

siRNAs corresponding to the TG mRNAs designed with 5′ phosphate, 3′ hydroxyl, and two base overhangs on each strand were synthesized and transfected to the ERα-positive VSMCs. The ERα-positive cells were seeded in a 25-cm^2 flask at an initial concentration of 50,000 cells/flask with F-12K medium containing 5% FBS and cultured until a subconfluent status was achieved. The medium was then replaced with phenol red-free and FBS-free medium to arrest the growth. After 24 hours, transfections of siRNA for endogenous gene targeting were performed with TransMessenger transfection reagent (Qiagen). The TG siRNA (2 μg per flask) was condensed with 4 μl of Enhancer R and formulated with 8 μl of TransMessenger reagent, according to the manufacturer's instructions. The transfection complex was added directly to the cells; it was replaced with phenol red-free medium containing 5% dextran-coated charcoal-stripped FBS (DCC-FBS) with E_2 (10 nmol/L), TAM (10 nmol/L), RAL (10 nmol/L), or vehicle (0.1% ethanol) after 3 hours. After incubation for 48 hours, we then measured the number of cells in each sample as described above. We also examined the number of cells treated with E_2 (10 nmol/L) or vehicle (0.1% ethanol) with transfection of negative control siRNA and treated by E_2 (10 nmol/L), TAM (10 nmol/L), RAL (10 nmol/L), or vehicle into both ERα-positive cells. After incubation for 48 hours, the cells were trypsinized and suspended. We then used Cell Counting Kit-8 system (Wako) for measurement of the number of cells in each sample. As a contrast, we also examined the number of cells treated with E_2 (10 nmol/L) or vehicle with transfection of TG or negative control siRNA in ERβ-positive cells treated by E_2. The effective ratio of transfection into the cells was more than 80% by using fluorescein-labeled negative control siRNA before transfection of the TG siRNA (data not shown). The sequence information of siRNA for TG is shown in Table 2.

Quantitative RT-PCR Analysis for mRNA of the TG Expression in Human Aorta

Human abdominal aortae without hormone therapy were collected at the time of autopsy performed in Tohoku University Hospital (Sendai, Japan) within 2 hours postmortem from 22 patients (6 male, 6 premenopausal female, 10 postmenopausal female; mean, 52.2 ± 5.9 years of age). The Ethics Committee at Tohoku University School of Medicine approved the research protocol for this study. Aortic specimens were tentatively classified into the following five groups as previously described,[25] A, B, C, D, and E based on the sex of the deceased patient, degree of atherosclerosis, and status of menstruation (group A: male, normal or mild atherosclerosis, corresponding to group I to III in the AHA classification; group B: male, advanced atherosclerosis, corresponding to group IV to VI in the AHA classification; group C: premenopausal female, normal or mild atherosclerosis; group D: postmenopausal female, advanced atherosclerosis; and group E: postmenopausal female, mild atherosclerosis). The distribution of the cases among these groups is summarized as follows: A, three cases; B, three cases; C, six cases; D, six cases; and E, four cases. The adventitia and fat tissues around the aorta were immediately and carefully removed using clean surgical scissors and forceps at the time of autopsy. After this procedure, these specimens were immediately frozen in liquid nitrogen and stored at −80°C until use and also subsequently subjected to total RNA extraction for real-time RT-PCR analysis described above for expression levels of TG product mRNA and the correlation of ERα mRNA abundance in those samples. The mRNA levels for target product and ERα in each sample are summarized as a ratio of GAPDH, and evaluated as a ratio (%) compared with that of each control cDNA, which were synthesized from each PCR product and purified by using the pGEM-T Easy vector, as described above.

In Situ *Hybridization Study for the TG mRNA Expression in Human Aorta*

Unstained and duplicated, 5-μm-thick, formalin-fixed, paraffin-embedded human aorta sections were mounted onto clear glass slides (Matsunami, Tokyo, Japan) and processed using the RiboMap *in situ* hybridization kit (Ventana Medical Systems, Tucson, AZ) on the Ventana Discovery (Ventana Medical Systems) automated *in situ* hybridization instrument. *In situ* hybridization step protocols after the deparaffinization step were designed based on the standard protocol described in the manufacture's RiboMap application note. The first fixation step was performed using formalin-based RiboPrep reagent (Ventana Medical Systems) for 30 minutes at 37°C. The reacted sections were then acid-treated using hydrochloride-based RiboClear reagent (Ventana Medical Systems) for 10 minutes at 37°C. The slides were subsequently processed for the protease digestion using ready-to-use a protease 2 reagent. The sections were incubated for hybridization with the anti-sense riboprobe (2 ng/slide) using RiboHybe hybridization buffer (Ventana Medical Systems) for 6 hours at 37°C after a denaturing step for 6 minutes at 70°C. After stringency wash step using 2× RiboWash (equivalent to 0.2× standard saline citrate, Ventana Medical Systems) for 6 minutes at 42°C, the second fixation step was performed using RiboFix reagent for 20 minutes at 37°C followed by incubation of biotin-labeled anti-digoxigenin antibody (Sigma) for 30 minutes at 37°C. After streptavidin-alkaline phosphatase conjugate incubation for 16 minutes at 37°C, the signal was detected automatically using the BlueMap NBT/BCIP substrate kit for 4 hours at 37°C. Finally, the sections were counterstained with Kernechtrot as a marker stain and covered with a glass coverslip. We also used double immunostaining with diaminobenzidine (DAB) for ERα using a monoclonal antibody (Novocastra Laboratories, Newcastle, UK) and Vector-blue for α-smooth muscle actin using a monoclonal antibody (DAKO Corp., Carpinteria, CA), respectively, in adjacent tissue sections to further characterize these positive cells in the human aorta of the cases positive for the target mRNAs. We also used a monoclonal antibody against CD31 antigen (DAKO) for endothelial cells and a monoclonal anti-human macrophage antibody (PG-M1, DAKO) for macrophages in adjacent tissue sections for further characterization. In addition, we performed labeling index (LI), a quantitative value that evaluates the number of TG mRNA-positive cells present in VSMCs of the aortic neointima and media.[24] After determining the areas of evaluation by simultaneous observation using a multiheaded light microscopy, three authors (T.S., M.S., and H.S.) independently evaluated 100 VSMCs. When interobserver differences were less than 5%, the mean value was determined as the LI. When interobserver differences were greater than 5%, the three aforementioned authors above re-evaluated the discrepant immunostained slides simultaneously using a multiheaded light microscope, after which the mean value was obtained. The sequence information of probes for *in situ* hybridization for TG is shown in Table 2.

Statistical Analysis

Values for all results are shown as mean ± SE of means (SEM). For comparisons between two groups, we used one-way analysis of variance followed by unpaired *t*-test. To examine the correlation of the two factors, we used a correlation coefficient (r) and a regression equation. A P value less than 0.05 was considered significant in this study.

Results

Characterization of Two VSMC Cell Lines

Results are summarized in Figures 1 and 2. We confirmed that these cells were positive for α-smooth muscle actin immunoreactivity but both of these cell lines represented relatively dedifferentiated VSMCs on the basis of their morphological features and expression of specific markers such as caldesmon, α-tropomyosin, and others (data not shown). In RT-PCR analysis, HUVS-112D cells

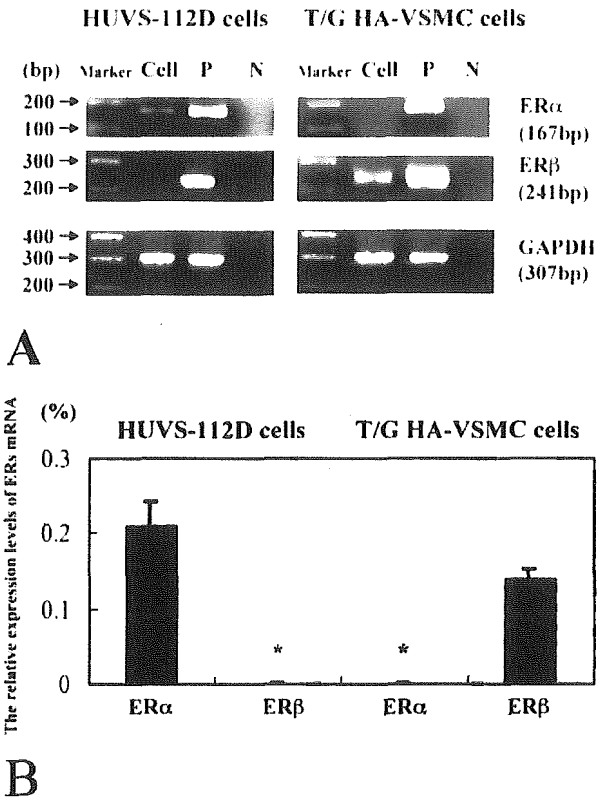

Figure 1. A: Results of real-time RT-PCR analysis for ERα and ERβ in two cultured human VSMC lines (HUVS-112D and T/G HA-VSMC), positive controls, and negative controls. Cell, each type of cultured VSMC; P, positive controls (T-47D breast cancer cell lines); N, negative controls (no cDNAs). T-47D breast cancer cell lines were both positive for ERα and ERβ. Negative controls yielded no bands for both ERα and ERβ. In HUVS-112D cells, only the bands of ERα were detected, whereas only the bands of ERβ were detected in T/G HA-VSMC cells. **B:** The relative mRNA expression levels for both ERs in two types of VSMC lines. The data for RT-PCR were adjusted by ratios (%) of GAPDH mRNA compared with that of each control cDNA, which were synthesized from each PCR product and purified by using the pGEM-T Easy vector. *, PCR products were not detected and the relative expression levels resulted in zero.

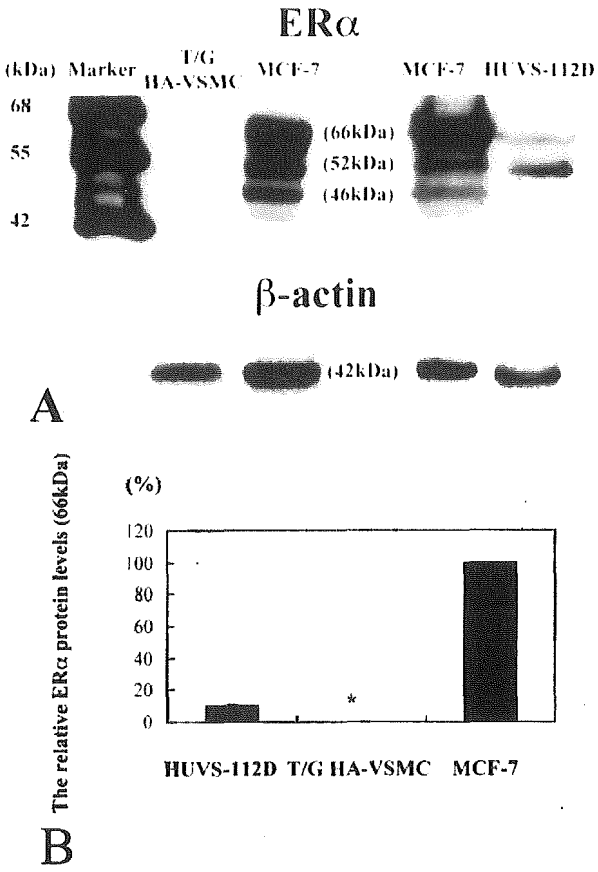

Figure 2. A: Western blot analysis of ERα and β-actin in HUVS-112D cells, T/G HA-VSMCs, and MCF-7 cells. Total protein was extracted and 60 μg of protein from each cell was loaded. Western blot analysis demonstrated both the full-length ERα protein (66 kd) in HUVS-112D and MCF-7 cells, but not in T/G HA-VSMCs. In addition, both HUVS-112D and MCF-7 cells were also positive for the exon 7 deletion variant of ERα protein (52 kd). On the other hand, MCF-7 cells were positive for another splicing variant of ERα protein (46 kd). **B:** The relative protein expression levels for the full-length ERα protein (66 kd) in two types of VSMC lines. The results were evaluated as a ratio (%) compared with that of untreated MCF-7 cells. *, Bands of protein were not detected and the relative expression levels resulted in zero.

were positive only for ERα (0.21 ± 0.03%, adjusted by ratios of GAPDH mRNA), and T/G HA-VSMCs were positive only for ERβ (0.14 ± 0.01%, adjusted by ratios of GAPDH mRNA) (Figure 1).

In Western blot analysis, only HUVS-112D cells were positive for the full-length ERα protein (66 kd) (10.4 ± 0.8%, adjusted by ratios of β-actin protein compared to the ratio of MCF-7 cells) (Figure 2). In addition, HUVS-112D cells were also positive for the exon 7 deletion variant of ERα protein (52 kd), which is known to be expressed in both human VSMCs and MCF-7 cells, and known to inhibit transcriptional activation of wild-type ERs with little transcriptional activity by itself (Figure 2).[25,26] On the other hand, MCF-7 cells were also positive for another splicing variant of ERα protein (46 kd) (Figure 2).[27]

Gene Chip Microarray Assay

Table 3 shows the 12 genes that demonstrated expression ratios of above 2.0 after 8 hours of duplicated 10 nmol/L E_2 treatment of ERα- and/or ERβ-positive cells. Among these genes, E4F transcription factor 1, ie, E4F1 was detected in HUVS-112D cells (ERα-positive cells), and its expression was associated with the second highest ratios by duplicated 10 nmol/L E_2 treatment (2.4-fold) (Table 3). In addition, among the detected genes, only E4F1 has been reported to inhibit cell growth and cell-cycle progression.[28–33] In addition, more than 20 half-EREs in the promoter region of E4F1 were detected in this search (data not shown). Therefore we further examined the features of E4F1 as an estrogen-responsive gene in human VSMCs and whether E4F1 was associated with estrogenic inhibition of ERα-positive cell proliferation using quantitative RT-PCR, and siRNA transfection assay described above. In addition, we examined the expression levels of E4F1 mRNA in human abdominal aorta using both quantitative RT-PCR and *in situ* hybridization. In this study, E4F1 was not detected in T/G HA-VSMC cells (ERβ-positive cells). In addition, among the genes detected by microarray analysis, the gene associated with inhibition of VSMC proliferation was not demon-

Table 3. Genes Up-Regulated by Estrogen Treatment for 8 Hours in Cultured VSMCs

Cell lines	Approved gene symbols	RefSeq accession numbers	Ratios
HUVS-112D (ERα-positive)	INPP4B	NM_003866	2.8
	E4F1	NM_004424	2.4
	CKLF	NM_016326	2.2
	RYR3	NM_001036	2.2
	PLAG1	NM_002655	2.1
T/G HA-VSMC (ERβ-positive)	RFP2	NM_005798	2.5
	CPM	NM_001874	2.4
	EGR3	NM_004430	2.3
	POFUT1	NM_015352	2.3
	ADPRTL2	NM_005484	2.1
	HAP1	NM_177977	2.1
	RBM12	NM_152838	2.1

Ratios represents the mean ratios of expression levels of each gene mRNA between biologically duplicated experiments with estrogen and without estrogen.

strated in ERβ-positive VSMCs according to the results of our research.

E4F1 mRNA Expression in VSMCs by Estrogen Treatment

E_2 significantly increased E4F1 mRNA levels of ERα-positive VSMCs compared to controls (131.9 ± 5.9% by E_2 100 pmol/L, 267.0 ± 19.7% by E_2 10 nmol/L, respectively; $P < 0.05$) (Figure 3A). In addition, E_2 with CHX also significantly increased those of ERα-positive VSMCs compared to controls (172.4 ± 20.3%, $P < 0.05$) (Figure 3A). However, E_2 with ICI 182780, TAM, RAL, and E_2 with ACD suppressed expression of these mRNAs (33.4 ± 0.1% by E_2 10 nmol/L with ICI 182780 1 μmol/L, 63.5 ± 16.9% by TAM 10 nmol/L, 32.3 ± 1.8% by RAL 10 nmol/L, 48.5 ± 10.6% by E_2 10 nmol/L with ACD 1 μmol/L, respectively; $P < 0.05$) (Figure 3A). In addition, E4F1 mRNA levels of ERα-positive VSMCs were the highest at 8 hours after E_2 10 nmol/L treatment compared to control (267.0 ± 19.7%) (Figure 3C). However, none of E_2 significantly increased or inhibited E4F1 mRNA levels of ERβ-positive VSMCs compared to controls (Figure 3, B and D). In summary, results of quantitative RT-PCR analyses also demonstrated that E4F1 is one of the genes induced by estrogen via ERα, but not via ERβ, in our cultured human VSMCs.

E4F1 siRNA Transfections and Cell Proliferation Assay

We confirmed the down-regulation of E4F1 mRNA levels in the cells by transfection of E4F1 siRNAs using RT-PCR (data not shown). After transfection of negative control siRNA, all E_2 and estrogen receptor modulators (SERMs) used in this study significantly inhibited proliferation of ERα-positive VSMCs compared to controls (20.0 ± 2.2% by E_2 10 nmol/L, 28.2 ± 1.0% by TAM 10 nmol/L, and 12.0 ± 0.2% by RAL 10 nmol/L, respectively; $P < 0.05$) (Figure 4A). In addition, TAM and RAL significantly inhibited proliferation of ERα-positive VSMCs compared to controls (30.7 ± 1.6% by TAM 10 nmol/L, and 13.7 ± 1.0% by RAL 10 nmol/L, respectively; $P < 0.05$) after transfection of E4F1 siRNA (Figure 4A). However, E_2 with transfection of E4F1 siRNA did not suppress the proliferation of ERα-positive VSMCs (Figure 4A). In addition, none of the agents examined in this study significantly inhibited the cell proliferation of ERβ-positive VSMCs compared to controls by transfection of both E4F1 siRNA and negative control siRNA (Figure 4B). In summary, siRNA analysis indicated that E4F1 may be associated with inhibition of VSMC proliferation through ERα not ERβ in our cultured VSMCs.

E4F1 mRNA Expression in Human Aorta

The relative abundance of E4F1 mRNA determined by real-time PCR analysis was significantly higher in the premenopausal female aorta with a mild degree of atherosclerotic changes (group C, 2.22 ± 0.37%) than in the male aorta with a mild degree of atherosclerosis (group A, 0.09 ± 0.05%), with a severe degree of atherosclerosis (group B, 0.31 ± 0.27%), and in the postmenopausal female aorta with a severe degree of atherosclerosis (group D, 0.24 ± 0.12%) ($P < 0.05$) (Figure 5B). In addition, there was a significant positive correlation between expression levels of ERα mRNA and relative abundance of E4F1 mRNA expression in female aorta ($y = 0.571 + 1.641 * x$, $r = 0.65$; $P < 0.05$) (Figure 5C). In addition, there was a significant inversed correlation between ages of the patients and the abundance of E4F1 mRNA expression in female aorta ($y = 2.482 - 0.026 * x$, $r = -0.575$; $P < 0.05$) (data not shown). However, no significant correlations were detected between relative abundance of E4F1 mRNA and ages and degree of atherosclerosis in male aorta (data not shown). In summary, results of quantitative RT-PCR in human aorta demonstrated that E4F1 was markedly expressed in premenopausal female aorta in an early stage of atherosclerosis with abundant ERα.

In Situ *Hybridization Study for E4F1 mRNA Expression in Human Aorta*

Expression of E4F1 mRNA products were markedly present in ERα-positive VSMCs at neointima of aorta in

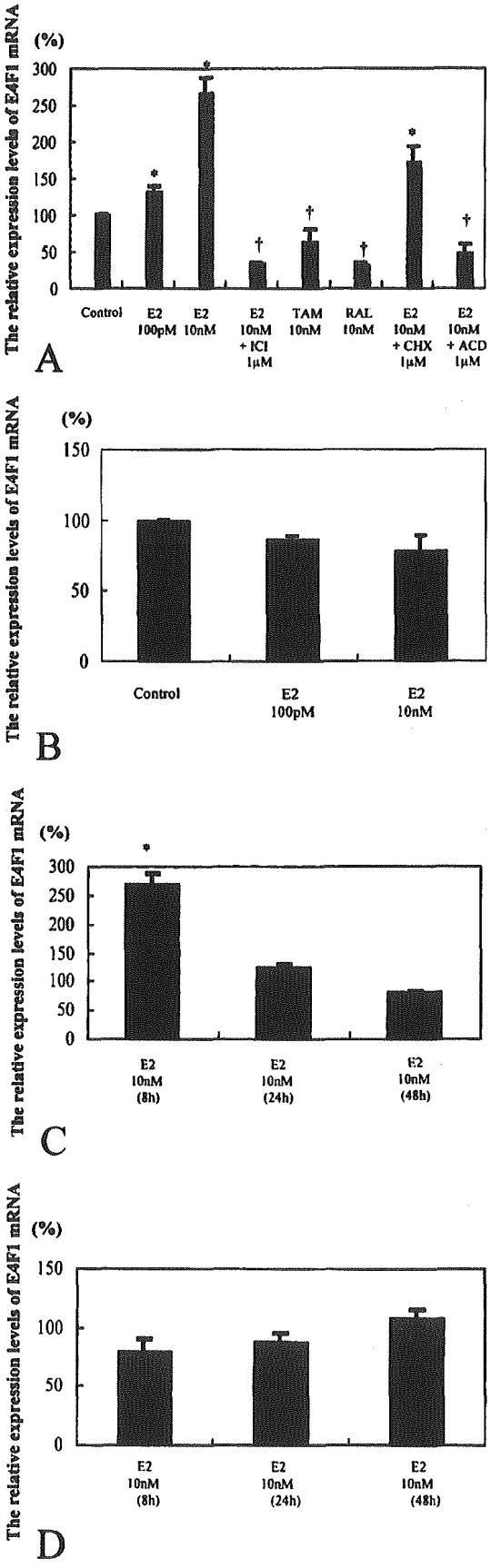

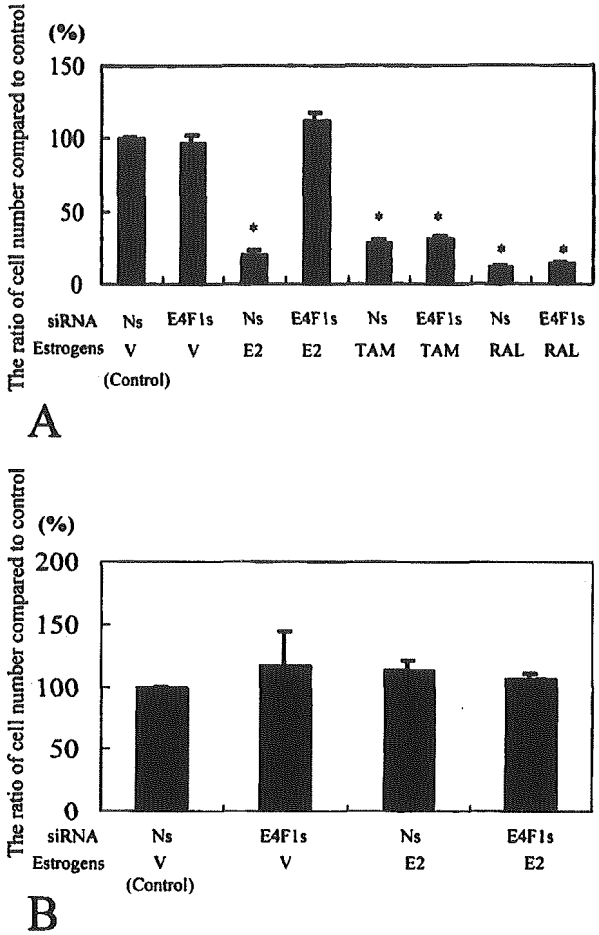

Figure 4. A: The relative levels of cell numbers in HUVS-112D cells (ERα-positive cells) among cells treated with vehicle (control), estrogen (E_2) alone (10 nmol/L), tamoxifen (TAM; 10 nmol/L), raloxifene (RAL; 10 nmol/L), or vehicle (V; 0.1% ethanol) after transfection of E4F1 siRNA (E4F1s) or negative control siRNA (Ns). *, Significantly decreased compared to control; $P < 0.05$. **B:** The relative levels of cell numbers in T/G HA-VSMCs (ERβ-positive cells) among cells treated with vehicle (control), E_2 alone (10 nmol/L), or vehicle (V; 0.1% ethanol) after transfection of E4F1 siRNA (E4F1s) or negative control siRNA (Ns). *, Significantly decreased compared to control; $P < 0.05$.

group C. However, a very low level of expression of both E4F1 mRNA and ERα immunoreactivity was demonstrated in the nuclei of VSMCs of aorta in other groups. In addition, none of CD31-positive cells or PG-M1-positive cells demonstrated any hybridization signals of E4F1 mRNAs (data not shown). Figure 6 shows representative illustrations of an abdominal aorta specimen obtained from a 38-year-old woman with a mild degree of athero-

Figure 3. A: Results of real-time RT-PCR analysis for E4F1 in HUVS-112D cells (ERα-positive cells) among cells treated with vehicle (control), E_2 alone (100 pmol/L, 10 nmol/L), E_2 (10 nmol/L) with ICI 182780 (1 μmol/L), E_2 (10 nmol/L) with actinomycin D (ACD; 1 μmol/L), E_2 (10 nmol/L) with cycloheximide (CHX; 1 μmol/L), tamoxifen (TAM) alone (10 nmol/L), and raloxifene (RAL) alone (10 nmol/L), respectively, after 8 hours. **B:** Results of real-time RT-PCR analysis for E4F1 in T/G HA-VSMCs (ERβ-positive cells) among cells treated with vehicle (control), E_2 (100 pmol/L, 10 nmol/L) alone, respectively, after 8 hours. **C** and **D:** The relative levels of E4F1 mRNA expression in ERα-positive cells (**C**) and ERβ-positive cells (**D**) treated by E_2 alone (10 nmol/L) after 8, 24, and 48 hours compared to control (treated by vehicle). *, Significantly increased compared to control; †, significantly decreased compared to control; $P < 0.05$.

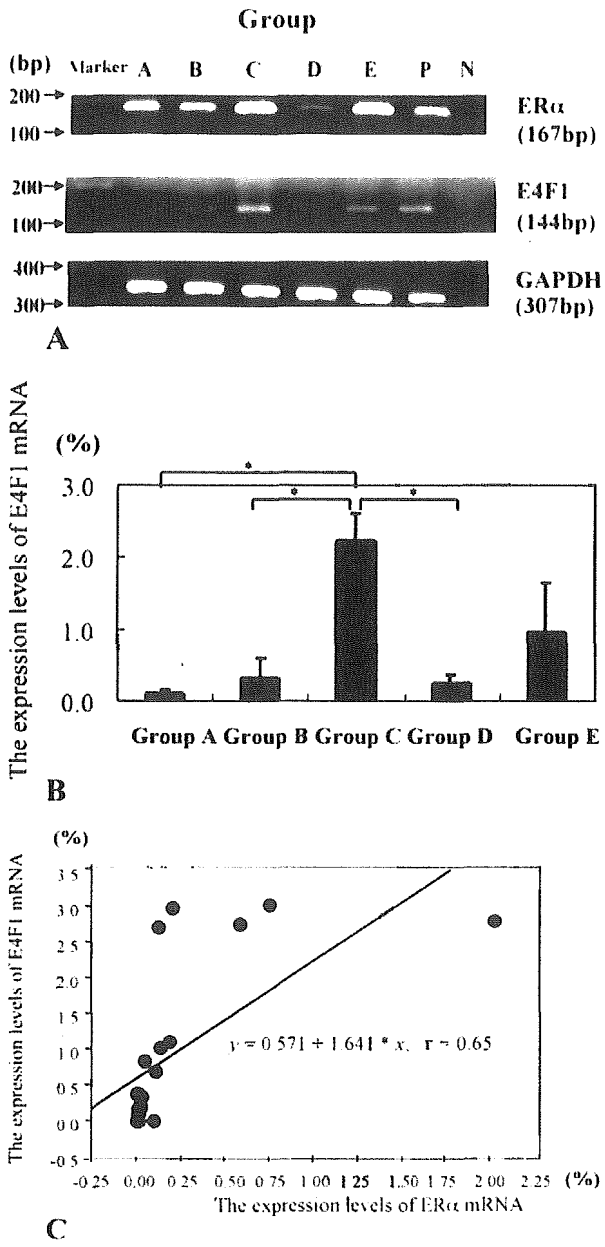

Figure 5. A: Results of real-time RT-PCR analysis for E4F1 in human aortas. Bands for PCR products were detected as specific single bands (167 bp for ERα, 144 bp for E4F1, and 307 bp for GAPDH). The amplified products were run on a 2% agarose gel stained with ethidium bromide. Representative photographs for these real-time RT-PCR gene products are illustrated. A, Aorta of a 32-year-old man with mild atherosclerotic change; B, Aorta of a 65-year-old man with severe atherosclerotic change; C, aorta of a 38-year-old premenopausal woman with mild atherosclerotic change; D, aorta of a 76-year-old postmenopausal woman with severe atherosclerotic change; E, aorta of a 71-year-old postmenopausal woman with mild atherosclerotic change; P, positive controls; N, negative controls. **B:** The results for mRNA expression levels for E4F1 ($P < 0.05$). **C:** Correlation between the levels of mRNA expression for ERα and E4F1 in 22 samples of human aorta. A significant correlation was detected ($y = 0.571 + 1.641x$; $r = 0.65$; $P < 0.05$).

sclerosis (group C). The number of E4F1 mRNA-positive cells in the neointima was significantly higher in the premenopausal female aorta with a mild degree of atherosclerotic changes (group C, 24.0 ± 2.0 LI) than in the male aorta with a mild degree of atherosclerosis (group A, 5.6 ± 0.5 LI), in the male aorta with a severe degree of atherosclerosis (group B, 3.2 ± 0.4 LI), in the postmenopausal aorta with a severe degree of atherosclerosis (group D, 2.4 ± 0.5 LI), and in the postmenopausal aorta with a mild degree of atherosclerosis (group E, 6.2 ± 1.5 LI) ($P < 0.05$) (Table 4). However, LI for E4F1 mRNAs in the media was not significantly different among these groups (Table 4). In summary, results of *in situ* hybridization study in human aorta demonstrated that E4F1 was markedly expressed in ERα-positive VSMCs present at neointima of premenopausal female aorta in an early stage of atherosclerosis.

Discussion

In this study, results of microarray and quantitative RT-PCR analyses all suggest that E4F1 is one of the genes induced by estrogen via ERα, but not via ERβ, in cultured human VSMCs. In addition, siRNA analysis demonstrated that E4F1 might be associated with inhibition of VSMC proliferation through ERα. Results of quantitative RT-PCR and *in situ* hybridization studies in human aorta further showed that E4F1 was markedly expressed in ERα-positive VSMCs present at neointima of premenopausal female aorta in an early stage of atherosclerosis.

In this study, we used duplicated microarray analyses as an initial screening. We then confirmed whether the gene was induced by estrogens or not by triplicated (using three flasks per treatment or nontreatment) quantitative RT-PCR. We then used siRNA assay for further examination of the findings. These findings all demonstrated that results of microarray analysis were consistent with those of RT-PCR, and the gene revealed by microarray analysis was actually involved in estrogenic inhibition of ERα-positive VSMC proliferation as demonstrated by the cell count assay with siRNA transfection.

E4F1 is well-known as a Krüppel-like family member.[28] The growth inhibitory activity of E4F1 has also been demonstrated to be associated with the posttranscriptional elevation of several cell-cycle regulatory proteins, including the CDK inhibitors $p21^{Waf1}$ and $p27^{Kip1}$ with reduced cdk2 and cdk4/6 activities, and with the down-regulation of cyclin A and cyclin E gene expression.[28–30] E4F1-induced cell-cycle arrest has been also reported to be enhanced by its interaction with the p53 transcription factor and hypophosphorylated pRb.[28,32,33] All of these findings above are consistent with the results of previous studies reported, and with inhibitory effects of estrogens on VSMC proliferation.[34]

Stimulation of responsive genes in response to estrogen is postulated to be mediated by the direct binding in which E_2-liganded ER binds directly to a specific sequence called an ERE and interacts directly with coactivator proteins and components of the RNA polymerase II transcription initiation complex which result in enhanced transcription.[35] This is also consistent with results of our computer-based search of ERE in the promoter region of E4F1. In addition, quantitative RT-PCR analysis in our present study also demonstrated that ACD suppressed estrogen-induced E4F1 mRNA expression,

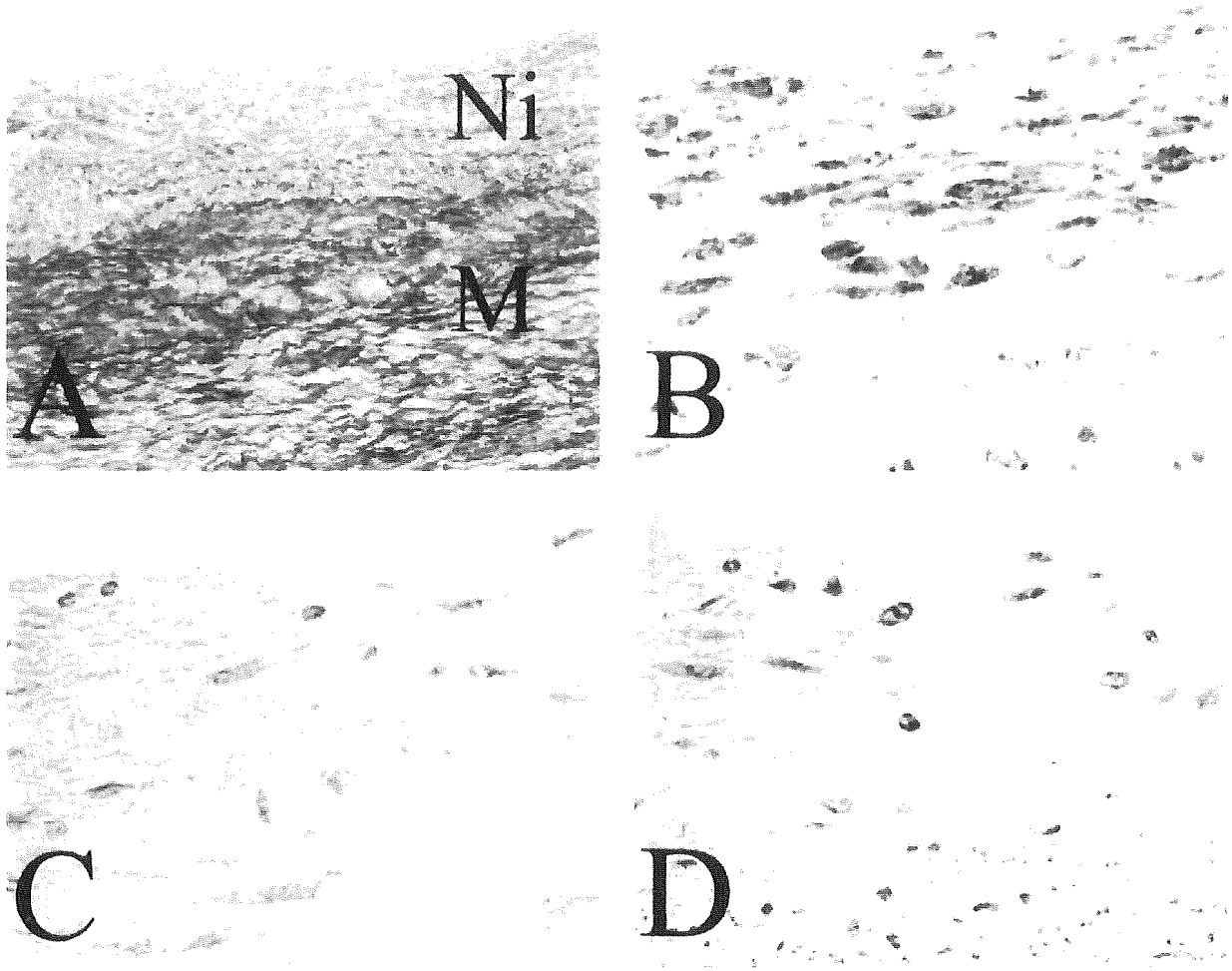

Figure 6. Modified Masson-Goldner's stains (**A**), double-immunohistochemical staining photos for α-smooth muscle actin and ERα in the neointima (**B**), and *in situ* hybridization of E4F1 mRNA in the neointima (**C** and **D**) of an abdominal aorta specimen obtained from a 38-year-old premenopausal woman with a mild degree of atherosclerosis (group C). **B:** Immunopositive cells for ERα appear brown as a result of diaminobenzidine colorimetric reaction. Immunopositive cells for α-smooth muscle actin appear blue as a result of Vector-blue colorimetric reaction. Double-immunopositive cells are confirmed. **C:** Negative control hybridized with sense oligonucleotide probes showed no detectable specific mRNA hybridization signals. Nuclear staining, appearing red, was performed by Kernechrot. **D:** E4F1 mRNA hybridization signals, appearing blue, were detected in the marginal region of VSMCs in the neointima. Nuclear staining, appearing red, was performed by Kernechrot. Ni, neointima; M, media. Original magnifications: ×100 (**A**); ×400 (**B–D**).

but CHX did not inhibit its expression. Therefore, these findings all indicated that E4F1 is considered one of the first established responsive genes in ERα-positive VSMCs. However, it is not known whether these half-EREs are associated with estrogenic actions or not.

Table 4. Results of Labeling Index (LI) for Target Gene (E4F1) mRNAs in VSMCs of Human Aorta

Group	*n*	Neointima	Media
Group A	3	5.6 ± 0.5	2.0 ± 0.5
Group B	3	3.2 ± 0.4 *	2.0 ± 0.4
Group C	6	24.0 ± 2.0 *	4.8 ± 1.0
Group D	6	2.4 ± 0.5 *	3.4 ± 0.7
Group E	4	6.2 ± 1.5	4.8 ± 0.7
Total	22	7.3 ± 1.8	3.4 ± 0.4

Data are the mean ± SEM. A statistical significance was evaluated among the groups using one-way analysis of variance followed by unpaired *t*-test.
* $P < 0.05$.

Therefore, it awaits further investigation for clarification to detect a strict E4F1 promoter region and then to demonstrate whether ERα is actually binding to each ERE present at upstream region of E4F1 promoter using a chromatin immunoprecipitation assay.[36,37]

Results of our study in human aorta also demonstrated that levels of E4F1 mRNA expression were significantly higher in VSMCs of neointima of premenopausal female aorta with mild atherosclerotic changes than in those of other groups. This finding therefore suggests that E4F1 is mainly expressed in dedifferentiated/proliferating VSMCs positive for ERα in neointima of premenopausal female aorta. This finding also demonstrated that the expression of E4F1 may be strongly induced by estrogens via ERα in VSMCs present at neointima of those aorta, possibly involved in inhibitory actions of VSMC proliferation by estrogens to prevent neointimal formation.[38]

SERMs are postulated to be an attractive alternative with respect to cardiovascular risk reduction, providing

that they exert cardioprotective effects like estrogens. SERMs act as ER antagonists in the breast and uterus, avoiding the harmful effects of estrogens but presumably preserving the beneficial effects of estrogens on bone, lipids, and the cardiovascular system.[39–41] In addition, it is known that TAM binds with similar affinity to both ERs, whereas RAL has a higher affinity for ERα.[42,43] Moreover, a previous report demonstrated that TAM has partial agonist activities on anti-atherogenic effects and vascular reactivity through interaction with ERα but not with ERβ in human VSMCs.[9] These all may be consistent with results of our present study. It is also postulated that estrogenic effects by SERMs are induced through AP-1 pathway.[35] However, several previous reports also documented that pretreatment of SERMs blocked the anti-atherogenic effects exerted by E_2 and that they have mixed estrogenic and anti-estrogenic effects on anti-atherogenesis in VSMCs and endothelial cells.[44–46] Both TAM and RAL are reported to inhibit the classical ERE pathway described above activated by E_2 when these cells are treated together with E_2 and SERMs,[35] which is also consistent with these above reports.[44–46] Results of quantitative RT-PCR and cell proliferation studies also demonstrated that E4F1 was induced by estrogens and suppressed the cell proliferation in ERα-positive VSMCs, but not by TAM or RAL, which may be partially consistent with results of these above reports. Therefore, SERMs may also be involved in inhibition of ERα-positive VSMC proliferation not through the above classical pathway induced by E4F1 based on results of our present investigations. These results all suggest the possible involvement of other pathways of estrogenic inhibition of VSMC proliferation. This may be also consistent with a previous report demonstrating that SERMs exert an anti-proliferative effect in VSMCs, at least in part through a p38 cascade whose activation is mediated by ERα via a nongenomic mechanism.[47] However, further investigations are required to determine how these above pathways interact with each other in estrogenic and/or anti-estrogenic effects on VSMCs, and to examine whether there are other possible pathways involved in estrogenic anti-atherogenic processes in human VSMCs *in vivo*, including an analysis of the difference between E_2 and SERMs.

In our study, estrogens demonstrated no inhibitory effects in proliferation of ERβ-positive VSMCs. In addition, results of our present study also demonstrated that the inhibitory actions of VSMC proliferation via E4F1 were not detected in these VSMCs, whereas ERβ was reported to be predominantly expressed in VSMCs.[9] Furthermore, ERβ has recently been demonstrated not only to play an essential role in the regulation of vascular function and blood pressure, but also to be associated with several mechanisms of anti-atherogenic effects.[48–50] These previous reports of *in vitro* studies all suggest that E_2 was associated with growth inhibitory actions in porcine and/or rat VSMCs predominantly through ERβ stimulation.[50,51] The signaling pathway mediating growth inhibition via ERβ has been also reported to be through reduction of p42/44 and p38 MAPK activity, and/or the cyclic AMP-adenosine pathway.[49–52] These signaling pathways may be attributable to the nongenomic action of E_2.[53,54] However, ERβ is well-known as a relatively less potent transactivator than ERα at low receptor concentrations, such as in our T/G HA-VSMC cell lines, in response to E_2.[9] This may be one of the reasons to explain the absence of an inhibitory role of estrogenic signals via ERβ on VSMC proliferation demonstrated in our present study. ERβ is also reported to predominantly increase after injury to the carotid artery of rat, and may be also consistent with promoting inhibitory actions through increment of ERβ concentrations.[55] On the other hand, previous studies on vascular injury using fully null ERα knockouts indicated that ERα is basically and predominantly important for anti-atherogenic effects of estrogen in mice, which is consistent with results of our present study.[13] However, according to these several previously published reports, it is difficult to exclude the possibility that which ER is more important for anti-atherogenesis depends on difference of species. Therefore, it still remains unclear which subtype of ER is more important for estrogenic anti-atherogenic effects in human, although our present study demonstrated the above pathway through ERα and E4F1. In addition, all previous reports have demonstrated several pathways of estrogen-induced anti-atherogenic effects *in vitro* but not *in vivo*, and therefore it remains unclear which pathway is most important for ERα-mediated anti-atherogenic effects *in vivo*. Further investigations in atherosclerotic models or in human cardiovascular system are required for clarification.

In conclusion, E4F1 is considered one of the estrogen-responsive genes involving ERα-mediated inhibition of VSMC proliferation and may play important roles in estrogen-related atheroprotection of human aorta.

Acknowledgment

We thank Naomi Kanai for technical assistance.

References

1. Stampfer MJ, Colditz GA, Willett WC, Manson JE, Rosner B, Speizer FE, Hennekens CH: Postmenopausal estrogen therapy and cardiovascular disease. N Engl J Med 1991, 325:756–762
2. Viscoli C, Brass L, Kernan W, Sarrel P, Suissa S, Horowitz R: A clinical trial of estrogen-replacement therapy after ischemic stroke. N Engl J Med 2001, 345:1243–1249
3. Rossouw JE, Anderson GL, Prentice RL, LaCroix AZ, Kooperberg C, Stefanick ML, Jackson BD, Beresford SA, Howard BV, Johnson KC, Kotchen JM, Ockere J: Writing Group for the Women's Health Initiative Investigators: Risk and benefits of estrogen plus progestin in healthy postmenopausal women. Principal results from the Women's Health Initiative randomized controlled trial. JAMA 2002, 288:321–333
4. Hulley S, Furberg C, Barrett-Connor E, Cauley J, Grady D, Haskell W, Knopp R, Lowery M, Satterfield S, Schrott H, Vittinghoff E, Hunninghake D: HERS Research Group. Noncardiovascular disease outcomes during 6.8 years of hormone therapy. HERS II. JAMA 2002, 288:58–66
5. Sullivan TR, Karas RH, Aronovitz M, Faller GT, Ziar JP, Smith JJ, O'Donnell TF, Mendelson ME: Estrogen inhibits the response-to-injury in a mouse carotid artery model. J Clin Invest 1995, 96:2482–2488
6. Hodgin JB, Krege JH, Reddick RL, Korach KS, Smithies O, Maeda N: Estrogen receptor α is a major mediator of 17β-estradiol's anti-atherogenic effects on lesion size in Apoe $^{-/-}$ mice. J Clin Invest 2001, 107:333–340
7. Kuiper GG, Enmark E, Pelto-Huikko M, Nillson S, Gustafsson JÅ:

Cloning of a novel receptor expressed in rat prostate and ovary. Proc Natl Acad Sci USA 1996, 93:5925–5930
8. Kuiper GG, Carlsson B, Grandien K, Enmark E, Haggblad J, Nilsson S, Gustafsson JÅ: Comparison of the ligand binding specificity and transcript tissue distribution of estrogen receptor α and β. Endocrinology 1997, 138:863–870
9. Hodges YK, Tung L, Yan XD, Graham JD, Horwitz KB, Horwitz LD: Estrogen receptors α and β: prevalence of estrogen receptor β mRNA in human vascular smooth muscle and transcriptional effects. Circulation 2000, 101:1792–1798
10. Brouchet L, Krust A, Dupont S, Chambon P, Bayard F, Arnal JF: Estradiol accelerates reendothelialization in mouse carotid artery through estrogen receptor-α but not estrogen receptor-β. Circulation 2001, 103:423–428
11. Losordo DW, Kearney M, Kim EA, Jekanowski J, Isner JM: Variable expression of the estrogen receptor in normal and atherosclerotic coronary arteries of premenopausal women. Circulation 1994, 89: 1501–1510
12. Sudhir K, Chou TM, Chatterje K, Smith EP, Williams TC, Kane JP, Malloy MJ, Korach KS, Rubanyi GM: Premature coronary artery disease associated with a disruptive mutation in the estrogen receptor gene in a man. Circulation 1997, 96:3774–3777
13. Pare G, Krust A, Karas RH, Dupont S, Aronovitz M, Chambon P, Mendelsohn ME: Estrogen receptor-alpha mediates the protective effects of estrogen against vascular injury. Circ Res 2002, 90:1087–1092
14. Gruvberger S, Ringner M, Chen Y, Panavally S, Saal LH, Borg A, Ferno M, Peterson C, Meltzer PS: Estrogen receptor status in breast cancer is associated with remarkably distinct gene expression patterns. Cancer Res 2001, 61:5979–5984
15. Soulez M, Parker MG: Identification of novel oestrogen receptor target genes in human ZR75-1 breast cancer cells by expression profiling. J Mol Endocrinol 2001, 27:259–274
16. Krichevsky AM, Kosik KS: RNAi functions in cultured mammalian neurons. Proc Natl Acad Sci USA 2002, 99:11926–11929
17. Park WS, Kurosaki MN, Hayafune M, Nakajima E, Matsuzaki T, Shimada F, Takaku H: Prevention of HIV-1 infection in human peripheral blood mononuclear cells by specific RNA interference. Nucleic Acids Res 2002, 30:4830–4835
18. Wilda M, Fuchs U, Wossmann W, Borkhardt A: Killing of leukemic cells with a BCR/ABL fusion gene by RNA interference (RNAi). Oncogene 2002, 21:5716–5724
19. Vladusic EA, Hornby AE, Guerra-Vladusic FK, Lakins J, Lupu R: Expression and regulation of estrogen receptor beta in human breast tumors and cell lines. Oncol Rep 2000, 7:157–167
20. Nakamura Y, Miki Y, Suzuki T, Nakata T, Darnel AD, Moriya T, Tazawa C, Saito H, Ishibashi T, Takahashi S, Yamada S, Sasano H: Steroid sulfatase and estrogen sulfotransferase in the atherosclerotic human aorta. Am J Pathol 2003, 163:1329–1339
21. Kondo E, Horii A, Fukushige S: The human PMS2L proteins do not interact with hMLH1, a major DNA mismatch repair protein. J Biochem (Tokyo) 1999, 125:818–825
22. Guzeloglu-Kayisli O, Kayisli UA, Al-Rejjal R, Zheng W, Luleci G, Arici A: Regulation of PTEN (phosphatase and tensin homolog deleted on chromosome 10) expression by estradiol and progesterone in human endometrium. J Clin Endocrinol Metab 2003, 88:5017–5026
23. Watanabe H, Suzuki A, Kobayashi M, Lubahn DB, Handa H, Iguchi T: Similarities and differences in uterine gene expression patterns caused by treatment with physiological and non-physiological estrogens. Mol Endocrinol 2003, 31:487–497
24. Konishi H, Steinbach G, Terry NH, Lee JJ, Dubin JA, Glober GA, Fujita K, Spaulding D, Cass L, Hittelman WN: Histone H3 messenger RNA in situ hybridization correlates with in vivo bromodeoxyuridine labeling of S-phase cells in rat colonic epithelium. Cancer Res 1996, 56:434–437
25. Mompeo B, Tscheuschilsuren G, Aust G, Metz S, Spanel-Borowski K: Estrogen receptor expression and synthesis in the human internal thoracic artery. Ann Anat 2003, 185:57–65
26. Garcia Pedrero JM, Zuazua P, Martinez-Campa C, Lazo PS, Ramos S: The naturally occurring variant of estrogen receptor (ER) ERDeltaE7 suppresses estrogen-dependent transcriptional activation by both wild-type ERalpha and ERbeta. Endocrinology 2003, 144:2967–2976
27. Flouriot G, Brand H, Denger S, Metivier R, Kos M, Reid G, Sonntag-Buck V, Gannon F: Identification of a new isoform of the human estrogen receptor-alpha (hER-alpha) that is encoded by distinct transcripts and that is able to repress hER-alpha activation function 1. EMBO J 2000, 19:4688–4700
28. Rizos H, Diefenbach E, Badhwar P, Woodruff S, Becker TM, Rooney RJ, Kefford RF: Association of p14ARF with the p120E4F transcriptional repressor enhances cell cycle inhibition. J Biol Chem 2003, 278:4981–4989
29. Fajas L, Paul C, Vie A, Estrach S, Medema R, Blanchard JM, Sardet C, Vignais ML: Cyclin A is a mediator of p120E4F-dependent cell cycle arrest in G1. Mol Cell Biol 2001, 21:2956–2966
30. Fernandes ER, Zhang JY, Rooney RJ: Adenovirus E1A-regulated transcription factor p120E4F inhibits cell growth and induces the stabilization of the cdk inhibitor p21WAF1. Mol Cell Biol 1998, 18: 459–467
31. Rooney RJ: Cell cycle attenuation by p120E4F is accompanied by increased mitotic dysfunction. Cell Growth Differ 2001, 12:505–516
32. Sandy P, Gostissa M, Fogal V, Cecco LD, Szalay K, Rooney RJ, Schneider C, Del Sal G: p53 is involved in the p120E4F-mediated growth arrest. Oncogene 2000, 19:188–199
33. Fajas L, Paul C, Zugasti O, Le Cam L, Polanowska J, Fabbrizio E, Medema R, Vignais ML, Sardet C: pRB binds to and modulates the transrepressing activity of the E1A-regulated transcription factor p120E4F. Proc Natl Acad Sci USA 2000, 97:7738–7743
34. Dzau VJ, Braun-Dullaeus RC, Sedding DG: Vascular proliferation and atherosclerosis: new perspectives and therapeutic strategies. Nat Med 2002, 8:1249–1256
35. Paech K, Webb P, Kuiper GG, Nilsson S, Gustafsson JÅ, Kushner PJ, Scanlan TS: Differential ligand activation of estrogen receptors ERalpha and ERbeta at AP1 sites. Science 1997, 277:1508–1510
36. Metivier R, Penot G, Hubner MR, Reid G, Brand H, Kos M, Gannon F: Estrogen receptor-alpha directs ordered, cyclical, and combinatorial recruitment of cofactors on a natural target promoter. Cell 2003, 115:751–763
37. Oesterreich S, Deng W, Jiang S, Cui X, Ivanova M, Schiff R, Kang K, Hadsell DL, Behrens J, Lee AV: Estrogen-mediated down-regulation of E-cadherin in breast cancer cells. Cancer Res 2003, 63:5203–5208
38. Ross R: The pathogenesis of atherosclerosis: a perspective for the 1990s. Nature 1993, 362:801–809
39. Mitlak BH, Cohen FJ: Selective estrogen receptor modulators: a look ahead. Drugs 1999, 57:653–663
40. Weryha G, Pascal-Vigneron V, Klein M, Leclere J: Selective estrogen receptor modulators. Curr Opin Rheumatol 1999, 11:301–306
41. Goldfrank D, Haytoglu T, Frishman WH, Mohammad Z: Raloxifene, a new selective estrogen receptor modulator. J Clin Pharmacol 1999, 39:767–774
42. Mendelsohn ME, Karas RH: The protective effects of estrogen on the cardiovascular system. N Engl J Med 1999, 340:1801–1811
43. Gruber CJ, Tschugguel W, Schneeberger C, Huber JC: Production and actions of estrogens. N Engl J Med 2002, 346:343–352
44. Mikkola TS, Clarkson TB: Estrogen replacement therapy, atherosclerosis, and vascular function. Cardiovasc Res 2002, 53:605–619
45. Espinosa E, Oemar BS, Luscher TF: 17 Beta-estradiol and smooth muscle cell proliferation in aortic cells of male and female rats. Biochem Biophys Res Commun 1996, 221:8–14
46. Somjen D, Knoll E, Kohen F, Stern N: Effects of phytoestrogens on DNA synthesis and creatine kinase activity in vascular cells. Am J Hypertens 2001, 14:1256–1262
47. Mori-Abe A, Tsutsumi S, Takahashi K, Toya M, Yoshida M, Du B, Kawagoe J, Nakahara K, Takahashi T, Ohmichi M, Kurachi H: Estrogen and raloxifene induce apoptosis by activating p38 mitogen-activated protein kinase cascade in synthetic vascular smooth muscle cells. J Endocrinol 2003, 178:417–426
48. Zhu Y, Bian Z, Lu P, Karas RH, Bao L, Cox D, Hodgin J, Shaul PW, Thorén P, Smithies O, Gustafsson JÅ, Mendelsohn ME: Abnormal vascular function and hypertension in mice deficient in estrogen receptor β. Science 2002, 295:505–508
49. Watanabe T, Akishita M, Nakaoka T, Kozaki K, Miyahara Y, He H, Ohike Y, Ogita T, Inoue S, Muramatsu M, Yamashita N, Ouchi Y: Estrogen receptor beta mediates the inhibitory effect of estradiol on vascular smooth muscle cell proliferation. Cardiovasc Res 2003, 59: 734–744
50. Geraldes P, Sirois MG, Tanguay JF: Specific contribution of estrogen

receptors on mitogen-activated protein kinase pathways and vascular cell activation. Circ Res 2003, 93:399–405
51. Geraldes P, Sirois MG, Bernatchez PN, Tanguay JF: Estrogen regulation of endothelial and smooth muscle cell migration and proliferation: role of p38 and p42/44 mitogen-activated protein kinase. Arterioscler Thromb Vasc Biol 2002, 22:1585–1590
52. Dubey RK, Gillespie DG, Mi Z, Rosselli M, Keller PJ, Jackson EK: Estradiol inhibits smooth muscle cell growth in part by activating the cAMP-adenosine pathway. Hypertension 2000, 35:262–266
53. Morey AK, Pedram A, Razandi M, Prins BA, Hu RM, Biesiada E, Levin ER: Estrogen and progesterone inhibit vascular smooth muscle proliferation. Endocrinology 1997, 138:3330–3339
54. Takeda-Matsubara Y, Nakagami H, Iwai M, Cui TX, Shiuchi T, Akishita M, Nahmias C, Ito M, Horiuchi M: Estrogen activates phosphatases and antagonizes growth-promoting effect of angiotensin II. Hypertension 2002, 39:41–45
55. Lindner V, Kim SK, Karas RH, Kuiper GG, Gustafsson JA, Mendelsohn ME: Increased expression of estrogen receptor-beta mRNA in male blood vessels after vascular injury. Circ Res 1998, 83: 224–229
56. Pujol P, Rey JM, Nirde P, Roger P, Gastaldi M, Laffargue F, Rochefort H, Maudelonde T: Differential expression of estrogen receptor-alpha and -beta messenger RNAs as a potential marker of ovarian carcinogenesis. Cancer Res 1998, 58:5367–5373
57. Moore JT, McKee DD, Slentz-Kesler K, Moore LB, Jones SA, Horne EL, Su JL, Kliewer SA, Lehmann JM, Willson TM: Cloning and characterization of human estrogen receptor beta isoforms. Biochem Biophys Res Commun 1998, 247:75–78
58. Tokunaga K, Nakamura Y, Sakata K, Fujimori K, Ohkubo M, Sawada K, Sakiyama S: Enhanced expression of a glyceraldehyde-3-phosphate dehydrogenase gene in human lung cancers. Cancer Res 1987, 47:5616–5619